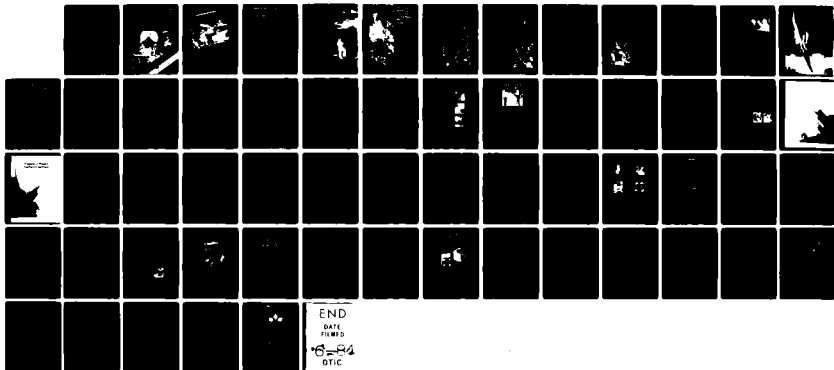


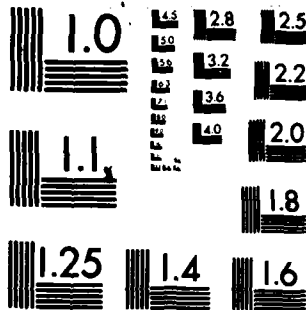
AD-A140 555 NAVAL RESEARCH REVIEWS VOLUME 35 NUMBER 3(U) OFFICE OF 1/1  
NAVAL RESEARCH ARLINGTON VA W J LESCURE 1983

UNCLASSIFIED

F/G 5/2

NL





MICROCOPY RESOLUTION TEST CHART  
NATIONAL BUREAU OF STANDARDS-1963-A

# Naval Research Reviews

Office of Naval Research  
Three/1983  
Vol XXXV

AD-A140 555

APPROVED FOR PUBLIC RELEASE  
DISTRIBUTION UNLIMITED

①



DTIC FILE COPY

DTIC  
ELECTE  
APR 25 1984  
S D  
B

84 04 06 166

Special Issue  
The Naval Weapons Center

Navy ordnancemen  
and civilian engineers load an 11.5-inch  
forward-firing aircraft rocket, "Tiny Tim," on aircraft  
for test firing in 1944.



Navy ordnancemen and civilian engineers load an 11.75-inch forward-firing aircraft rocket, "Tiny Tim," on aircraft for test firing in 1944. Tiny Tim was developed at China Lake late in World War II for use against German V-1 launching sites in France. Although progress of the war precluded the weapon's use in Europe, Tiny Tim was used in combat at Okinawa. Tiny Tim was developed as part of the wartime rocket program carried on at the Naval Ordnance Test Station (now the Naval Weapons Center (NWC)) under the leadership of the California Institute of Technology. That effort yielded such highly successful combat weapons as the 3.5-inch rocket, the 5-inch rocket, and the 5-inch high-velocity aircraft rocket ("Holy Moses"); an entire family of spin stabilized barrage rockets; and the facilities for research, development, test, and evaluation of propellants, explosives, warheads, and airframes that formed the foundations of the future NWC complex.

# Naval Research Reviews

Office of Naval Research  
Three/1983  
Vol XXXV

## Articles

- Tectonics, Seismicity, and Volcanism at the Naval Weapons Center by Glenn R. Roquemore and John T. Zellmer **3**
- Ramjet Combustion Instability Research by James E. Crump, Klaus C. Schadow, and H. Bernard Mathes **11**
- New Concepts for Thermal Batteries by M. H. Miles and A. N. Fletcher **19**
- Progress in Modern Explosives Synthesis by Ronald L. Atkins, Arnold T. Nielsen, Rodney L. Willer, and Richard A. Hollins **25**
- Surface Science with Photon-Stimulated Ion Desorption by Victor Rehn **36**
- The Michelson Laboratory Synchrotron Radiation Project by Victor Rehn **43**
- The Mathematics of Simple Random Walks by Daniel T. Gillespie **46**



## Departments

- Introductory Note by Dr. Edwin B. Royce **2**
- Research Notes **53**
- Profiles in Science—John Pearson **42**

### About the Cover

Naval fighter and attack aircraft soar past the masked and helmeted figure of a U.S. Navy aviator in a tribute to the dedication, skill, and versatility of the Navy pilot. Naval officers and enlisted men have always been an essential, integral part of the Naval Weapons Center's RDT&E efforts. The military-civilian team at the Center has operated for nearly 40 years with a single purpose: to provide the Fleet with effective, reliable tools with which to perform its mission. (Art work by William M. Erwin, NWC)

*Naval Research Reviews* publishes articles about research conducted by the laboratories and contractors of the Office of Naval Research and describes important naval experimental activities. Manuscripts submitted for publication, correspondence concerning prospective articles, and changes of address, should be directed to Code 732, Office of Naval Research, Arlington, Va. 22217. Requests for subscriptions should be directed to the Superintendent of Documents, U.S. Government Printing Office, Washington, D.C. 20402. *Naval Research Reviews* is published from appropriated funds by authority of the Office of Naval Research in accordance with Navy Publications and Printing Regulation NAVSO P-35.

Accession For	
NTIS GRA&I	<input checked="" type="checkbox"/>
DTIC TAB	<input type="checkbox"/>
Unannounced	<input type="checkbox"/>
Justification	
GPO-PRICE \$4.75	
By VOL. 35 No. 3, 1983	
Distribution/	
Availability Codes	
Dist	Avail and/or Special
A-124	



CHIEF OF NAVAL RESEARCH  
RADM L. S. Kollmorgen, USN

TECHNICAL DIRECTOR  
Dr. J. A. Smith

CHIEF WRITER/EDITOR  
W. J. Lescure, III

SCIENTIFIC EDITOR  
Dr. G. A. Neece

ASSOCIATE SCIENTIFIC EDITOR  
Dr. J. T. Lester

ASSOCIATE SCIENTIFIC EDITOR  
Dr. D. A. Paterson

MANAGING EDITOR  
M. J. Whetstone

ART DIRECTION  
Typography & Design  
Government Printing Office

## Introductory Note

Research has been a continuing part of the programs of the Naval Weapons Center from its earliest days. Today the Center's mission, involving air weapons and tactical missiles, requires the Center to maintain a broad program of research in physics, chemistry, mathematics, computer science, and the engineering sciences of detonation physics and aerothermochemistry. The articles in this issue of the *Naval Research Reviews* provide examples and summaries of some of the Center's research work.

Research efforts of the Naval Weapons Center are integrated with the Center's systems development activities. Thus, it is useful to view the program in terms of potential applications of its results.

The research program in physics is focused on optical, microwave, and electronic devices and materials. Applications of these efforts are in targeting, missile guidance, fuzing, and laser systems.

Research in chemistry encompasses a broad spectrum of applications, including optical and electronic materials, explosives, propellants, polymers, electrochemical devices for energy conversion applications, and instrumental analysis in support of all of these efforts.

Applications of efforts in mathematics and computer science include systems modeling and analysis, signal processing, control theory, stochastic processes, and applied artificial intelligence.

Explosives, warheads, and terminal effects are the subjects of interest in the research program in detonation physics, while missile propellants and propulsion systems are of interest in the aerothermochemistry research program.

Research scientists and engineers are generally given the freedom to explore research topics of their own choosing within this matrix of subjects, applications, and disciplines. While the Center's research program is not large, it produces annually some 50 to 60 refereed publications and a similar number of presentations. Funding support for the program comes primarily from the Naval Material Command, the Office of Naval Research, the naval systems commands, and the Defense Advanced Research Projects Agency.

Dr. Edwin B. Royce  
Head, Research Department  
Naval Weapons Center





# Tectonics, Seismicity, and Volcanism at The Naval Weapons Center

by

Glenn R. Roquemore  
and  
John T. Zellmer  
Naval Weapons Center

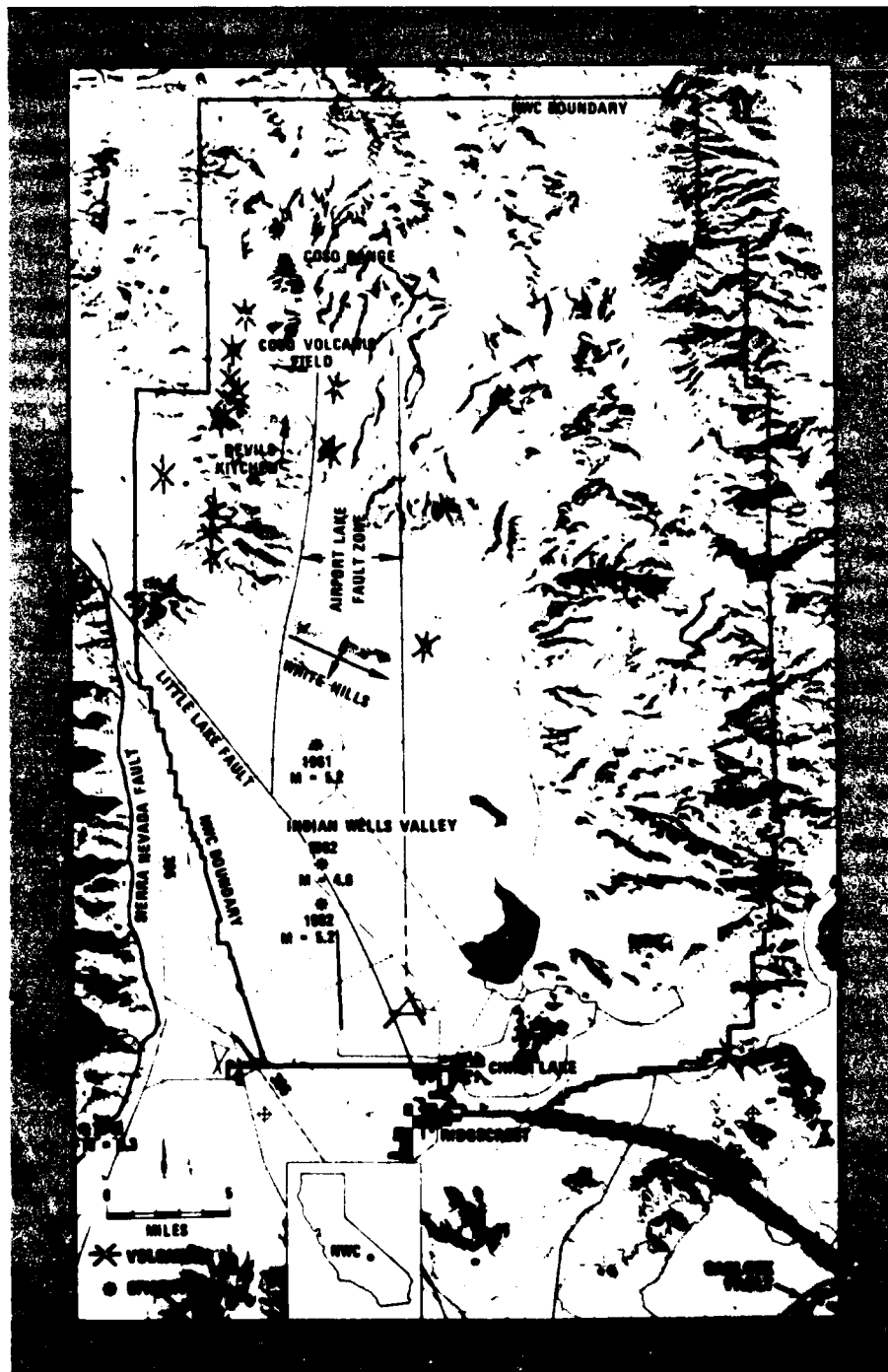
## Introduction

The Naval Weapons Center (NWC) at China Lake occupies a part of California known for its young geologic features and high level of seismic activity. The Coso Range and the Indian Wells Valley, which lie within the boundaries of NWC, are located in the southwestern corner of the Basin and Range physiographic province. The Coso Range encompasses 1,920 square kilometers; to the west is the Sierra Nevada, and to the east is the Argus Range. Owens Lake terminates the Coso Range to the north. The Indian Wells Valley covers 1,020 square kilometers to the south of the Coso Range (Figure 1). The largest population center and most of NWC's laboratory facilities are located in the Indian Wells Valley. This article describes the tectonics, seismicity, and volcanism of the Coso Range and the Indian Wells Valley, and the recent impacts that faulting, crustal deformation, and volcanic activity have had on NWC.

The Coso Range has a history of volcanism and earthquakes.

**Figure 1**

Index map of Coso Range and Indian Wells Valley, showing NWC, locations of volcanos, and epicenters of 1946 and 1961 earthquakes.



## The Coso Range

The Coso Range has a history of volcanism and earthquakes. The eruption of high-silica rhyolite occurred at least 38 times over the last million years, and basaltic eruptions ceased only 30,000 years ago. Duffield, *et al.*<sup>1</sup>, have shown that, in all, about 35 cubic kilometers of lava have erupted during the last 4 million years. The Coso Range has been broken by Basin and Range extensional faulting, as seen in the extensive horst and graben development and right-slip displacement. Bacon<sup>2</sup> has shown that the eruption of both basalt and rhyolite in the Coso Range has been controlled by regional tectonic extension.

Roquemore<sup>3</sup> has shown that earthquakes with magnitudes in the  $M = 8.0$  range may have occurred in the Coso Range within the last 1,600 years, and 0.5 meters of normal displacement along the Airport Lake fault probably occurred in 1872. Walter and Weaver<sup>4</sup> have reported that 4,800 earthquakes of  $M = 1.0$  to  $M = 3.9$  occurred within the Coso volcanic field from 1975 to 1977. Earthquakes of  $M \geq 5.0$  have occurred peripheral to the Coso Range. Some of these earthquakes include the 1872 Owens Valley earthquake ( $M = 8.3$ ) and the 1946 Walker's Pass earthquake ( $M = 6.3$ ). The majority of local earthquakes occurring within the Indian Wells Valley have been  $M \leq 5.2$ .

According to Combs<sup>5</sup>, the Coso Range contains abundant fumaroles, and high heat flow is associated with them. Teleseismic P-wave delays centered near the heat flow anomaly indicate a potential for partially melted material at a depth of between 8 and 20 kilometers. According to Reasenber, *et al.*<sup>6</sup>, an intense, low-velocity body is located under Devils Kitchen (Figure 2). This low-velocity body is approximately 5 kilometers wide on top and becomes increasingly elongated in the north-south, or  $N25^\circ E$  direction with depth. A maximum velocity contrast between the partially melted material and the surrounding rock is attained between 10 and 17.5 kilometers in depth. The heat source in the Coso volcanic field appears to be centered near Devils Kitchen.

Most of the dozens of known fumaroles in the Coso Range are associated with faults. Faults in the Coso Range that are associated with hot springs have significant components of normal slip. In general, these faults are segments of the Airport Lake fault zone and contain the highest concentration of hot springs in the region. Both the Airport Lake and the right-slip Little Lake faults have displacements and strikes consistent with the regional tectonic stress pattern.

**Figure 2**

Location of low-velocity body under Devils Kitchen.

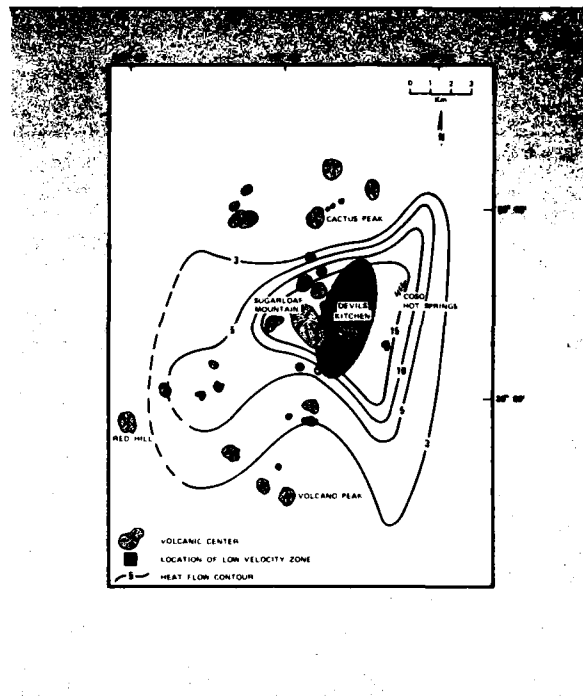


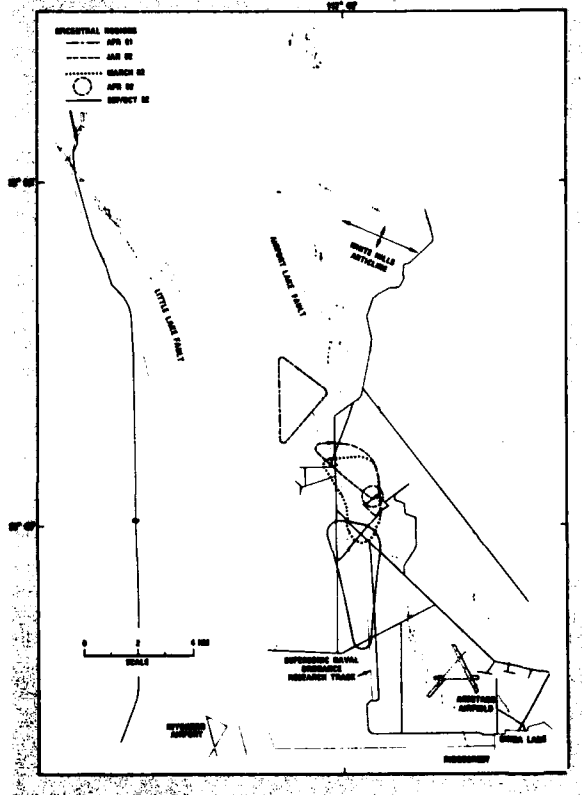
**Figure 3**

Aerial view of the Little Lake fault zone, showing typical geomorphic features and offset in a 400,000-year old basalt flow.



**Figure 4**

Locations of Airport Lake fault zone, Little Lake fault zone, and White Hills anticline.



## Little Lake and Airport Lake Faults

The Little Lake and Airport Lake faults are the two major active faults in the Indian Wells Valley and the Coso Range. These faults are components of the regional right-slip shear and the east-west extension that characterize the tectonics of the western Basin and Range physiographic province. The Little Lake and Airport Lake fault zones developed in response to the same regional tectonic stress field. Although these fault zones share a common origin, they represent different styles of deformation. The Little Lake fault is predominantly right slip, but develops a normal-slip component along its central and southern segments. It also has many geomorphic features similar to those of the San Andreas fault located on the western margin of California. The Airport Lake fault displays normal slip displacement and contains numerous nested grabens.

From the northwest corner of the Indian Wells Valley, the Little Lake fault splays southeast from the main trace of the Sierra Nevada frontal fault and trends diagonally across the valley to at least the NWC-Ridgecrest border. A seismic refraction study by Zbur<sup>7</sup> suggests that the bedrock expression of the Little Lake fault continues southward to the Garlock fault. The fault pattern is well-exposed on a basalt flow in the northwest part of the Indian Wells Valley (Figure 3). Rhombic depressions, pressure ridges, and linear troughs are typical along this portion of the fault. As the fault enters the deep alluvial basin of the Indian Wells Valley, its expression changes to short, segmented scarp traces that form an *en echelon* pattern.

The Airport Lake fault strikes north-south through the Coso Range and the Indian Wells Valley for over 35 kilometers (Figure 4). The northern segment of the fault is a narrow zone less than 0.5 kilometers wide. The central segment widens to 8 kilometers, forms Coso Basin, and extends into the Indian Wells Valley. Cinder cones, basaltic dikes, and symmetrically stepped grabens occur within the fault zone (Figure 5). The fault pattern bounding the zone is in places suggestive of oblique slip; however, within the fault zone the patterns are clearly normal slip and are associated with graben formation. Vertical displacement near Coso Valley totals at least 600 meters within a zone 5 kilometers wide.

The Little Lake and the Airport Lake faults intersect near the center of the Indian Wells Valley (Figure 4). This intersection is the locus of repeated seismic swarms that have been occurring since April 1981. Because of the high level and characteristics of seismicity and the notable changes in the surface expression of the faults, the intersection area has become the subject of much study. These changes suggest that much of the regional extension associated with the Airport Lake fault is being transferred to the Little Lake fault as right-slip displacement, both within and to the south of the zone of intersection.

## Geodetic and Level-Line Surveys

Survey data obtained at NWC's supersonic naval ordnance research track and within the geodetic and level-line trilateration network provide information about the regional and local tectonic stress fields and the related deformation occurring in the Coso Range and the Indian Wells Valley area. These data, in combination with tectonic studies such as those done by Wright<sup>8</sup>, indicate a regional stress field (Figure 4) resulting in right-slip shearing (evidenced in the Little Lake fault), extensional deformation (evidenced in the Airport Lake fault), and folding (evidenced in the White Hills anticline). Similar stress-related features on a smaller scale are also found in the Coso Range, in the Indian Wells Valley, and along the research track.

Periodic and highly precise surveys of the research track are used to maintain track alignment tolerances for supersonic rocket sleds. Surveys of the 7-kilometer-long research track and of Coso Range show that the region is actively deforming. Surveys suggest that between 1977 and 1978, the track uplifted 29 millimeters at its northern end and also may have

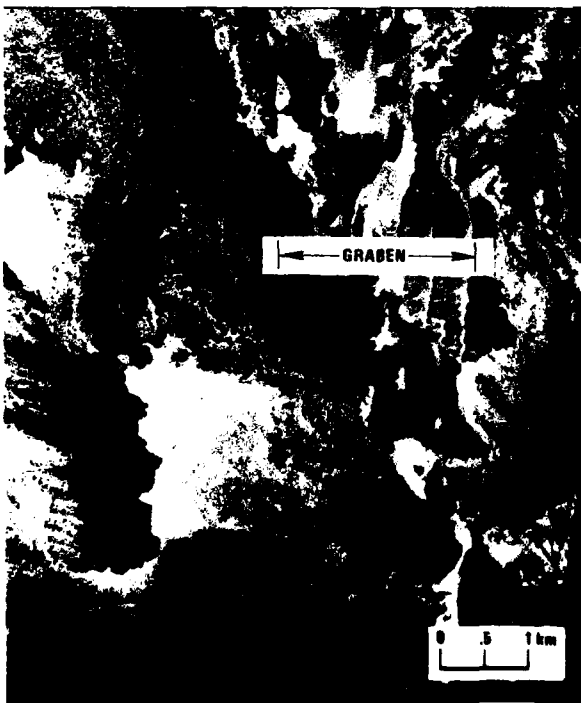
experienced minor lateral deformation and shortening. The track is being resurveyed to determine if additional deformations have occurred.

Repeated surveys in the Coso Range have included both leveling to detect elevation changes and trilateration to detect horizontal-slip displacements. On 13 March 1982 a possible spasmodic tremor (indicating volcanically induced seismic activity) was recognized near Cactus Peak in the Coso Range. To date, it is not known if the tremor actually occurred; however, several existing geodetic and level lines were resurveyed and new survey lines were added. Leveling surveys performed along a 20-kilometer-long line across the Coso volcanic field indicate that a 30-millimeter uplift occurred between 1975 and 1982. The result of the trilateration network surveys indicate that a slight north-south shortening and east-west lengthening may have occurred between 1975 and 1982. One hypothesis to explain the uplift and geodetic deformation along the track is that a sill of magma may have intruded into the upper crust. This hypothesis, proposed by Savage<sup>9</sup>, is being tested by continuing measurements and detailed studies of the earthquake data.

Because of the scientific interest generated by the earthquake swarms occurring since April 1981, the trilateration network was recently expanded to include 45 lines having a combined length of about 441 kilometers. The total area covered by the network is about 230 kilometers.

**Figure 5**

*Aerial view of the Airport Lake fault zone, showing a typical Graben.*



## Seismicity

The earthquake sequences that began during April 1981 marked the end of a 20-year period of seismic quiescence at NWC. The Indian Wells Valley area had not experienced any earthquakes of  $M \geq 4$  since 1961. During the period from April 1981 to October 1982, there were five earthquake sequences with maximum magnitudes ranging from  $M = 4.0$  to  $M = 5.2$  and several other sequences with earthquakes of lesser magnitude. These sequences contained 1,029 detectable earthquakes, 169 of which exceeded  $M = 2.5$  and 11 of which equaled or exceeded  $M = 4.0$ . The seismic record for the period of 1 December 1980 to 5 October 1982 is shown in Figure 6. Although the data set is complete only through 5 October 1982, a high number of low-magnitude earthquakes are still occurring as of December 1982.

The seismic record and the epicentral regions shown in Figure 4 indicate three general trends associated with the earthquake sequences. With each successive sequence, the tendency has been for the total number of earthquakes to increase, for the maximum magnitude to increase, and for the epicentral region to migrate southward. These sequences typically continue for several days or weeks. The first sequence, occurring in April 1981, contained five earthquakes and had a maximum magnitude of 4.0. The second sequence occurred in January 1982 and contained 8 earthquakes, the largest of which was  $M = 4.2$ . The third sequence, occurring in March



Higher levels of seismic activity can probably be expected to occur within this zone. Roquemore's analysis of paleoseismicity along the northern segment of the Little Lake fault suggests that earthquakes with magnitudes of  $M = 8.0$  or higher may have occurred within the last 1,600 years.

#### Future Concerns

If the volcanic field experienced spasmodic tremor and magmatic intrusion near Cactus Peak in the Coso Range, crustal adjustments (in the forms of earthquakes on the Little Lake and Airport Lake faults) may be relieving enough of the stress in the fault zone to allow for the propagation of magmatic dikes or sills toward the surface.

The recent earthquake sequences occurring in the Indian Wells Valley area and the trends exhibited by them are events that have not been observed before in this region. The relationship of these earthquakes to future seismic activity is not known. However, these events, in combination with the knowledge of the regional tectonic stress fields of the Indian Wells Valley area, have caused the U.S. Geological Survey and California Office of Emergency Services to jointly issue a warning that conditions may be favorable for earthquakes of larger magnitude ( $M \geq 5.2$ ) to occur within the year.

#### References

1. Duffield, W. A., C. R. Bacon and G. B. Dalrymple, "Late Cenozoic Volcanism, Geochronology and Structure of the Coso Range, Inyo County, California," *Journal of Geophysical Research*, 85:5 (1980) pp. 2381-2404.
2. Bacon, C. R., "Time-Predictable Bimodal Volcanism in the Coso Range, California," *Geology*, 10 (1982) pp. 65-69.
3. Roquemore, G. R., "Active Faults and Associated Tectonic Stress in the Coso Range, California," NWC TP 6270, Naval Weapons Center, China Lake, California (August 1981) 101 pp.
4. Walter, A. and C. S. Weaver, "Seismicity at the Coso Range, California," *Journal of Geophysical Research*, 85:5 (1980) pp. 2441-2458.
5. Combs, J., "Heat Flow in the Coso Geothermal Area, Inyo County, California," *Journal of Geophysical Research*, 85:5 (1980), pp. 2411-2424.
6. Reasenber, P. A., W. L. Ellsworth and A. W. Walter, "Teleseismic Evidence for a Low-Velocity Body Under the Coso Geothermal Area," *Journal of Geophysical Research*, 85:5 (1980) pp. 2471-2483.
7. Zbur, R. T., "A Geophysical Investigation of Indian Wells Valley, California," NOTS TP 2795, Naval Ordnance Test Station, China Lake, California (1963).
8. Wright, L., "Late Cenozoic Fault Patterns and Stress Fields in the Great Basin and Westward Displacement of the Sierra Nevada Block," *Geology*, 4 (1976) pp. 489-494.
9. Savage, J., "Deformation Surveys in the Coso Geothermal Area," USGS unpublished manuscript (1982).

#### Authors



Glenn R. Roquemore obtained his Ph.D. (Geology) at the University of Nevada, Reno, in 1981. He began working for the Naval Weapons Center as a summer hire in 1972 while a student at California State University, Fresno. Both his master's and PhD theses were on the geology and structure of the Coso Range. His recent work involves continental tectonics, especially earthquake and volcanic hazards to inland and coastal naval bases.

John T. Zellmer received his Ph.D. (Geology) from the University of Nevada, Reno, in 1981. He joined the NWC staff in 1982 as a research associate under a postdoctoral program sponsored by the National Research Council. His professional interests include neotectonics, geological engineering, and geologic hazards. A large portion of his academic and professional career has focused on the geology of the boundary region between the Basin and Range and Sierra Nevada physiographic provinces.



# Ramjet Combustion Instability Research

by

James E. Crump  
Klaus C. Schadow  
and  
H. Bernard Mathes  
Naval Weapons Center

## Introduction

The quest for military weapons of high accuracy at long standoff ranges has led to extensive research and development efforts to improve ramjet missile propulsion systems as well as other concepts that utilize the weight-saving fuel efficiencies possible through the use of airbreathing combustion systems. A part of the effort, which is under way at the Naval Weapons Center, involves research into methods for improving airbreathing combustion and thus increasing its viability for use in weapon systems. The studies described in this article are concerned with combustion instability in liquid fuel ramjet combustors.

Additional related research efforts are under way that deal with turbulent mixing and combustion in airbreathing systems such as gas generator ramjets (ducted rockets), solid fuel ramjets, and projectiles assisted by external burning drag reduction or thrust enhancement.<sup>1,6</sup> The knowledge gained from these efforts and from three decades of experience in solid propellant rocket motor combustion instability form a background of expertise for the studies described here.

## Combustion Instability in Ramjets

It is generally known that combustion-driven oscillations can occur in a wide variety of fuel-burning devices. Acoustic instability involves interactions between acoustic wave modes with the combustor and combustion processes in such a way that minor flow disturbances in the combustor gas are amplified into a standing acoustic wave. Acoustic instability in propulsion systems can interfere with missile performance, making instability a frequent problem in the design of propulsion systems. Such combustion-driven oscillations also occur in ramjet engines. In tests of ramjet engines of compact design, for example, low-frequency (100- to 500- Hz), combustion-induced, longitudinal pressure oscillations have been observed.<sup>7,8</sup> If these oscillations are of sufficiently high amplitude, they can cause inlet unstart and result in loss of engine performance.

Over the past 30 years, NWC has developed expertise in combustion instability in solid propellants. The goal of this research is to build a technology base to eliminate—or at least

control—instability so that acoustic pressure amplitudes can be lowered to acceptable levels. The progress of the effort in the solid propellant area has led to methods for testing the acoustic response of solid propellants and to the prediction of acoustic instability of solid propellant motors.<sup>9,10</sup> Experience gained from these studies, along with applications of high-frequency response instrumentation and data processing, has been communicated to members of the ramjet engine community.<sup>11,12</sup>

In recent studies of ramjet combustion instability, experimental and theoretical means were used to determine the relative importance of major combustor operational conditions on pressure oscillation amplitudes to ascertain the acoustic wave structure, to determine the shock oscillation properties, and to provide insight into shock and acoustic wave interaction. These experiments were performed in a coaxial dump combustor of simple design. Experiments to determine pressure wave structure in a more complex ramjet with side-mounted inlets (side dump) were also pursued, but are not reported here.<sup>13</sup>

## Experimental Arrangement

The laboratory-sized 5-in.-diameter heavy-walled ramjet combustor used in these studies is shown in Figure 1. Conditions for the majority of testing conducted to date are shown in Figure 2.

## Experimental Results and Interpretation

Research at NWC has concentrated on three major areas: (1) the effect of ramjet operational conditions on engine pressure oscillations,<sup>14</sup> (2) identification of acoustic modes that can be excited,<sup>15</sup> and (3) the response of the inlet shock to acoustic pressure oscillations in the inlet.<sup>16</sup> Another area of interest on which work has been initiated is interaction of the acoustic field with the coherent vortex structure generated in the shear layer near the plane of the dump and in the recirculation zone. (see Figure 1).

**Figure 1**

Arrangement of NWC research dump combustor.

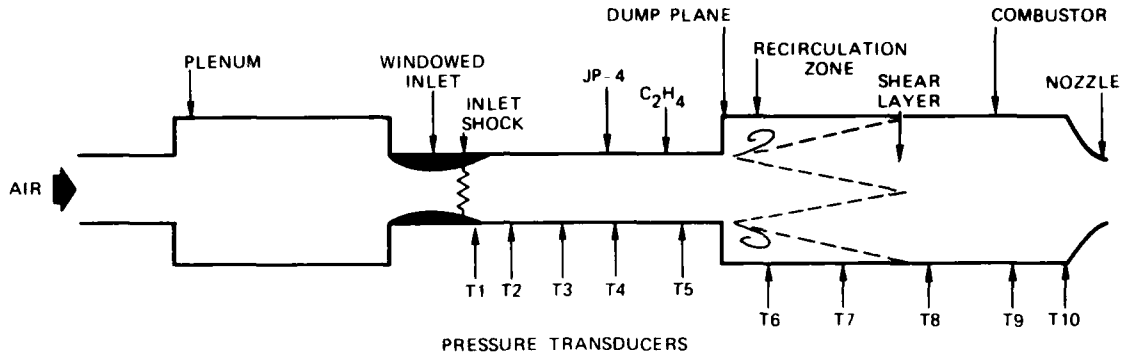
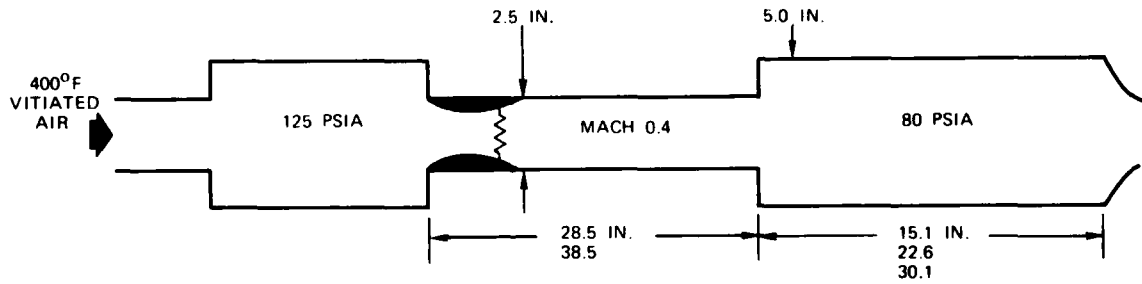


**Figure 2**

Test conditions.



AIR MASS FLOW: 5.0 LB/s  
C<sub>2</sub>H<sub>4</sub> MASS FLOW: 0.155 LB/s  
JP-4 MASS FLOW: 0.160 LB/s  
A/F (C<sub>2</sub>H<sub>4</sub>): 34/1  
A/F (JP-4): 30/1

### Effect of Operating Conditions

To be of maximum military use, a ramjet engine must operate over a range of speeds and altitudes. Those flight conditions result in changes of air mass flow at the inlet with related changes in air-to-fuel ratio, chamber pressure, and diffuser exit Mach number, all of which can affect combustion instability. In addition, design parameters such as engine geometry, type of fuel, fuel injection pattern, and fuel penetration into the inlet air flow can affect instability. Experiments at NWC have been designed to test the effects of those variables. One significant finding was that longitudinal acoustic instability was relatively insensitive to fuel type, permitting tests to be performed with a gaseous fuel (ethylene,  $C_2H_4$ ) rather than a liquid fuel (such as JP-4). On the other hand, optimum conditions for instability (highest acoustic amplitudes) were rather narrow, requiring 80 psia chamber pressure, a 5-lb/s inlet flow, and a diffuser exit Mach number of approximately 0.4.

One of the more significant results in terms of probable instability-driving mechanisms was the effect of fuel injection velocity (penetration into the inlet air flow) on the magnitude of the pressure oscillations (Figure 3). The injection velocity affects fuel entrainment, fuel mixing in the shear layer, and mixing and combustion in the recirculation zone (see Figure 1), which are of great importance in driving the combustion instability. This subject is under extensive investigation.

### Identification of Acoustic Modes

Structural characteristics of acoustic modes that can be generated in a ramjet are of considerable importance to instability research, particularly with regard to interactions between the acoustic wave and combustion and fluid dynamic processes in the engine. Mode identification is possible when numerous high-frequency-response pressure transducers are placed along the burner (T1 through T10, Figure 1). The oscillatory pressure data from the 10 transducers are recorded on multi-track magnetic tape. Data analysis consists of a series of tape playbacks in which the data are analyzed for frequency, amplitude, and phase. The results of a large number of tests in four different combinations of inlet length and combustor length (Table 1) have shown that:

1. Four different acoustic mode structures were generated.
2. More than one acoustic mode structure can be generated in a given engine configuration.
3. No unique relationship exists between a given mode structure and fuel type.

The results of the acoustic mode structure tests are summarized in Table 2. The third mode shape in that table (540 Hz) was observed in the majority of testing to date. Its characteristics were such that extensive test measurements were required

**Figure 3**

*Effect of fuel penetration.*

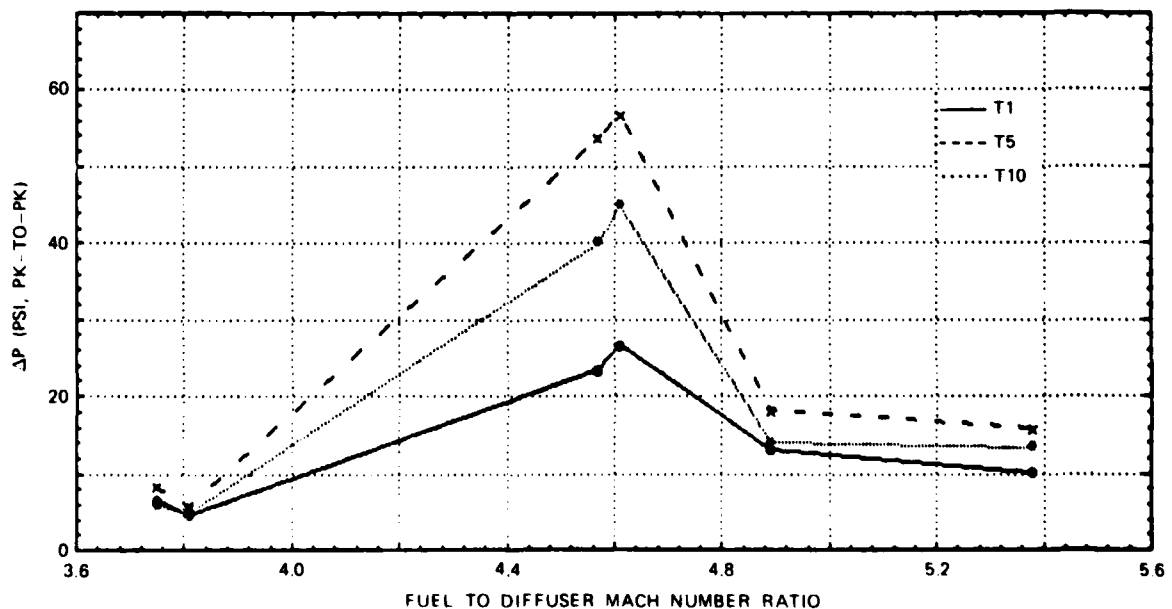


**Table 1***Ramjet Test Configurations.*

Configuration no. <sup>a</sup>	Length, in.	
	Inlet	Combustor
1	38.5	30.1
2	38.5	22.6
3	38.5	15.1
5	28.5	30.1

<sup>a</sup>Configuration No. 4 was not tested**Table 2***Observed Acoustic Modes*

MODE SHAPE	CONFIG	FREQ	FUEL
	NO. 1	175	- X -
	NO. 1	175	- X -
	NO. 2	190	X X X
	NO. 3	300	X X X
	NO. 1	540	X X
	NO. 1	540	X X
	NO. 5	540	X X
	NO. 2	650	X X

<sup>a</sup>Combustion mixture: combination of ethylene and JP-4. J  
JP-4

to verify its structure. The test measurements were also compared to analytical predictions of acoustic mode structure that are being conducted at the California Institute of Technology.<sup>17,18</sup>

The analytically predicted pressure amplitude of the third mode structure (Table 2) in the combustion chamber is approximately correct for a half-wave in a closed-closed organ pipe. In contrast, the waveform in the inlet shows the strong effects of both the shock and the mean flow. The latter causes a reduction of the wavelength, a result of the Doppler effect. The shock wave acts to absorb leftward-moving waves, a process which causes the waveform to move upstream during a cycle. This appears to be a traveling wave, as indicated in Figure 4, by plotting the curve at  $t=0$  and again, one-half cycle later. The pattern is repeated each cycle and is a reflection of the fact that the loss of acoustic energy at the shock wave introduces a constant phase shift between leftward and rightward moving waves and causes the reflected wave to have a smaller amplitude than the incident wave. The wave form can be characterized as a nonstationary, standing wave.

The pressure amplitude distributions in Figure 5 show good agreement between the experimental data (data points) and the analytical treatment (curve). In Figure 6, the relative phase of the oscillations (shown at a later time during one cycle than in Figure 5) are shown for both the analytical model (curve) and the experiment (data points). The correlation is good; the exact locations of the phase changes are different, but all the major features coincide.

In general, the acoustic mode data indicate that the mechanisms that cause longitudinal instabilities in the research dump combustor have a relatively broad band of responsiveness, since oscillations have been observed from as low as 170 Hz to as high as 650 Hz. Further details concerning results of NWC acoustic mode investigations will be found in References 19 and 20.

#### Response of Inlet Shock

In a series of tests to determine the response of the inlet shock to the oscillating diffuser exit pressure ( $P_{Dk}$ ) (540 Hz maximum), the oscillating inlet shock position, characterized by the diffuser area ratio (diffuser area at the shock position divided by area of the throat,  $A_{SH}/A_t$ ), was measured with Schlieren photography at 5,000 frames per second, and a time-average shock position was computed. With these experimental data the time-average shock Mach number and the time-average Mach number in the diffuser exit ( $M_{Dk}$ ) were calculated. By comparing these time-average experimental data with theoretical data based on one-dimensional isentropic theory and the dimensions of the ramjet inlet, the subsonic diffuser loss,  $\alpha$ , was determined as a function of  $M_{Dk}$ . The  $\alpha$  is defined as the diffuser exit pressure at stagnation divided by the diffuser pressure downstream of the shock at stagnation.

**Figure 4**

Analytical acoustic pressure amplitude for configuration No. 1 (540 Hz).

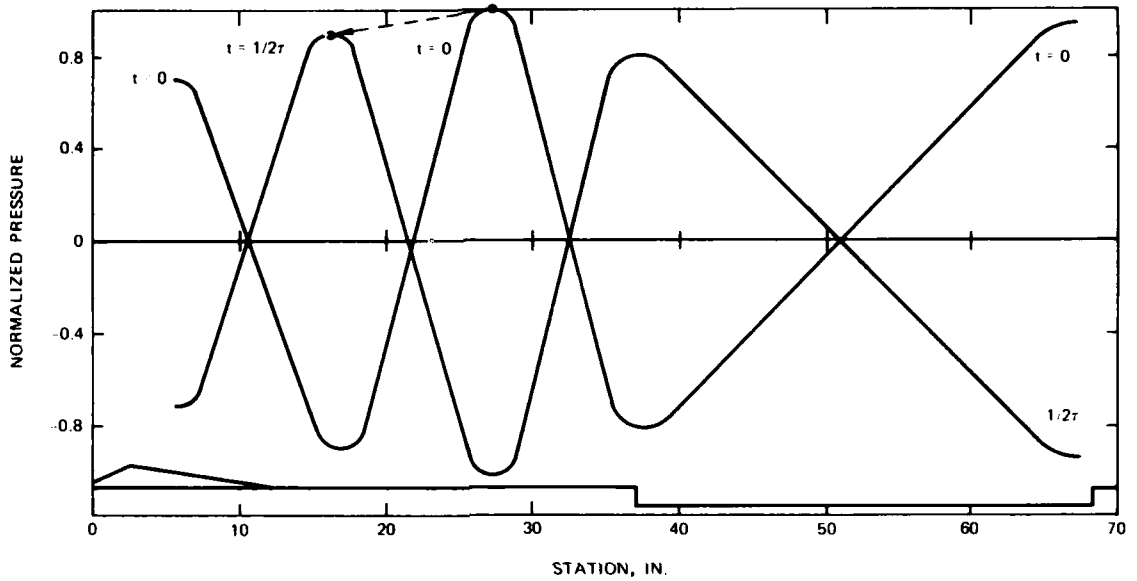


**Figure 5**

Acoustic pressure amplitude distribution.

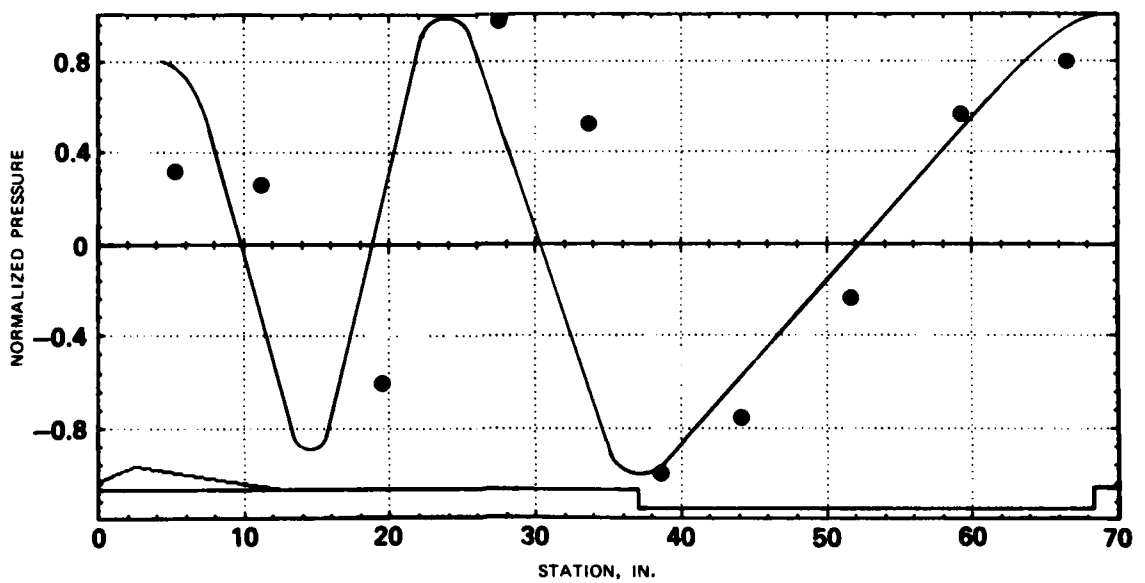


**Figure 6**

Relative phase of pressure oscillations.

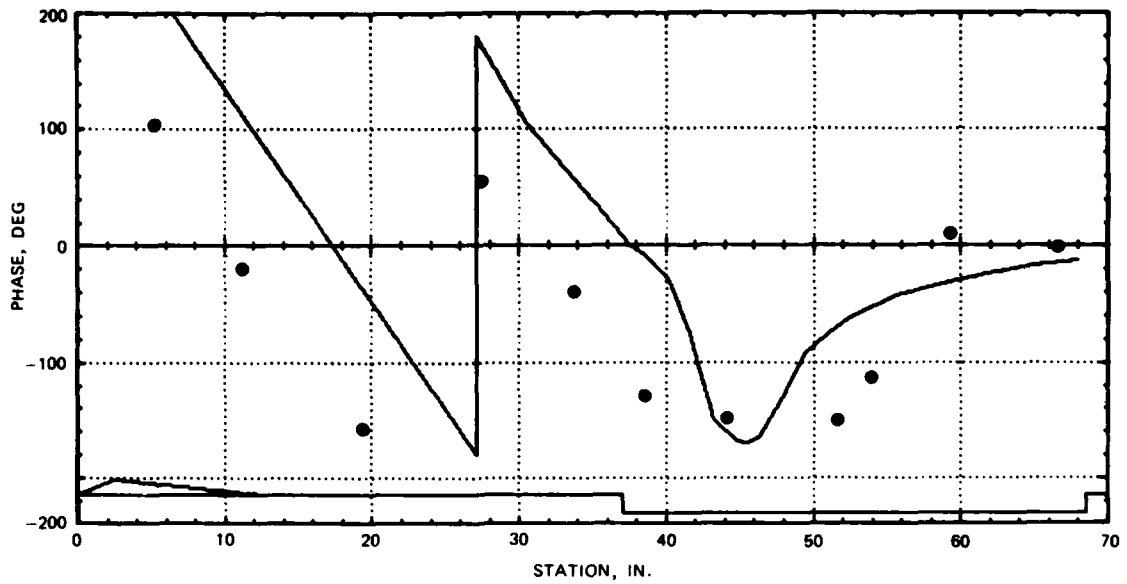
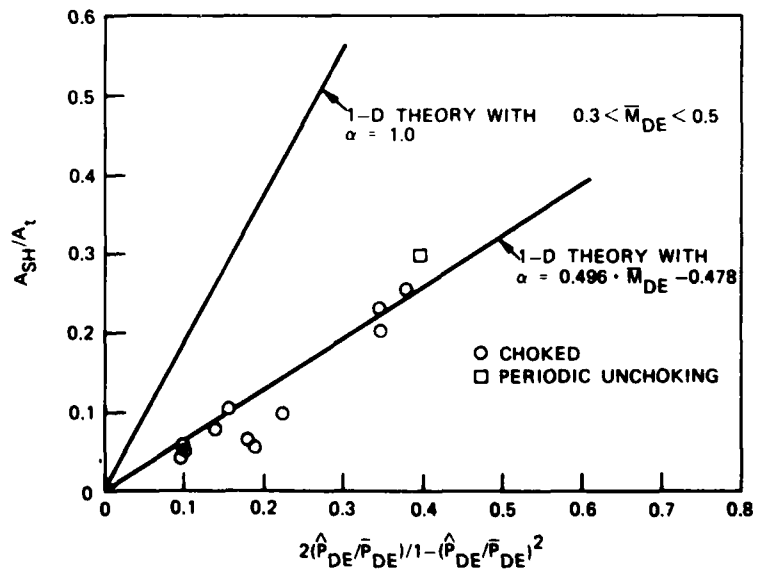


**Figure 7**

Shock displacement amplitude (peak-to-peak) versus diffuser exit pressure amplitude.



By applying  $\alpha$  determined for the steady-state conditions to the oscillatory conditions, good agreement was achieved between the theoretical shock displacement amplitudes (calculated from  $2(\bar{P}_{DE}/\bar{P}_{DE})/1 - (\bar{P}_{DE}/\bar{P}_{DE})^2$  with diffuser exit pressure amplitude,  $\bar{P}_{DE}$ , and mean value  $\bar{P}_{DE}$ ) and the experimental shock displacement amplitudes ( $\bar{A}_{SH}/A_i$ ) (determined from Schlieren photography) (Figure 7).<sup>21</sup> This agreement indicates that for the 540-Hz pressure oscillation the shock responded in a quasi-steady fashion to the pressure fluctuation amplitude.

## Summary

The results of the long-term program to determine the nature of acoustic combustion instability in ramjets have been encouraging. Predominant frequencies associated with acoustic modes of the ramjet cavity have been identified. Good agreement was achieved between experiments and theory for relative pressure amplitude and phase distribution in the ramjet cavity. It was found that droplet breakup/evaporative phase of liquid fuels is not a necessary condition for ramjet combustion instability. The relationship between inlet shock and diffuser exit pressure oscillations and the chamber acoustic modes and amplitudes has been described. Some effective applications of one-dimensional isentropic theory to calculate shock motion amplitude have been demonstrated. Pursuit of the implications of these and future findings should provide solutions to ramjet combustion instability and facilitate deployment of tactical ramjets.

## References

- Schadow, K. C., "Fuel-Rich, Particle-Laden Plume Combustion," *American Institute of Aeronautics and Astronautics Journal*, 13:12 (December 1975).
- Abbott, S. W., L. D. Smoot, and K. C. Schadow, "Direct Mixing and Combustion Efficiency Measurements in Ducted, Particle-Laden Jets," *American Institute of Aeronautics and Astronautics Journal*, 13:12 (March 1974) pp. 275-282.
- Schadow, K. C., "Boron Combustion in Ducted Rockets," *Proceedings of AGARD, London, England, October 1981*, CPP-307.
- Schadow, K. C., and D. J. Chieze, "Experimental Study on Base Drag Reduction with Combined Lateral and Axial Injection," *American Institute of Aeronautics and Astronautics Journal*, 16:10 (October 1978) pp. 1084-1089.
- Schadow, K. C., "Experimental Investigation of Combined External Burning/Base Burning," presented at the AIAA/SAE/ASME 16th Joint Propulsion Conference, Hartford, Connecticut, 30 June-2 July 1980, AIAA Preprint 80-1257.
- Schadow, K. C., H. F. Cordes, and D. J. Chieze, "Experimental Studies of Combustion Processes in a Tubular Combustor With Fuel Addition Along the Wall," *Combustion and Science Technology*, 19:1 (1978) pp. 51-57.
- Hall, P. H., "Response of Supercritical Inlets to Downstream Pressure Fluctuations," *Proceedings of AIAA/SAE/ASME 16th Joint Propulsion Conference, Hartford, Connecticut, 30 June-2 July 1980*, AIAA Paper 80-1118.
- Rogers, T., "Ramjet Inlet/Combustor Pulsations Analysis and Test," NWC TP 6155, Marquardt Company, China Lake, California, NWC (October 1980).
- Derr, R. L., H. B. Mathes, and J. E. Crump, "Application of Combustion Instability Research to Solid Propellant Rocket Motor Problems," presented at the AGARD 53rd Symposium on Solid Rocket Motor Technology, Oslo, Norway, 2-5 April 1979, *Conference Proceedings No. 259, Solid Rocket Motor Technology*, Neuilly-sur-Seine, France, Advisory Group for Aerospace Research and Development (1979) pp. 23-1 to 23-12.
- Mathes, H. B., "Assessment of Chamber Pressure Oscillations in the Shuttle Solid Rocket Booster Motor," presented at the AIAA/SAE/ASME 16th Joint Propulsion Conference, Hartford, Connecticut, 30 June-2 July 1980, AIAA Preprint No. 80-1091.
- Mathes, H. B., "Instrumentation for Measuring Pressure Oscillations," presented at the JANNAF Workshop on Pressure Oscillations in Ramjets, Monterey, California, September 1979.
- Mathes, H. B., "Techniques for Detecting and Analyzing Pressure Oscillations in a Research Dump Combustor," presented at the JANNAF Workshop on High Frequency Instrumentation and Data Analysis Techniques for Air-Breathing Combustors and Inlets, held in conjunction with the 1981 JANNAF Propulsion Meeting, New Orleans, Louisiana, 26-28 May 1981.
- Clark, W. H., "Static and Dynamic Performance Investigations of Side Dump Ramjet Combustors: Test Summary," NWC TP 6209, China Lake, California, NWC (December 1980).
- Schadow, K. C., J. E. Crump, R. L. Derr, and J. S. Heaser, "Studies of Pressure Oscillations in a Research Dump Combustor — A Progress Report," *Proceedings of the 17th JANNAF Combustion Meeting, Volume 1, Hampton, Virginia, 22-26 September 1980*, Chemical Propulsion Information Agency, Laurel, Maryland, 1980.

15. Crump, J. E., K. C. Schadow, F. S. Blomshield, and C. J. Bicker, "Combustion Instability in a Research Dump Combustor: Pressure Oscillations," *Proceedings of the 18th JANNAF Combustion Meeting, Pasadena, California, 19-23 October 1981*, Chemical Propulsion Information Agency, Laurel, Maryland, CPIA Publication, No. 347, 3(1981) pp. 357-370.

16. Schadow, K. C., J. E. Crump, and F. S. Blomshield, "Combustion Instability in a Research Dump Combustor: Inlet Shock Oscillations," *Proceedings of the 18th JANNAF Combustion Meeting, Pasadena, California, 19-23 October 1981*, Chemical Propulsion Information Agency, Laurel, Maryland, CPIA Publication No. 347, 3(1981) pp. 341-356.

17. Yang, V., and F. E. C. Culick, "Linear Theory of Pressure Oscillations in Liquid-Fueled Ramjet Engines," presented at the AIAA 21st Aerospace Sciences Meeting, Reno, Nevada, January 10-13, 1983, AIAA-83-0574.

18. Awad, E., and F. E. C. Culick, "Existence and Stability of Limit Cycles for Pressure Oscillations in Combustion Chambers," presented at the AIAA 21st Aerospace Sciences Meeting, Reno, Nevada, January 10-13, 1983, AIAA-83-0576.

19. Culick, F. E. C., and T. Rogers, "The Response of Normal Shocks in Inlet Diffusers," presented at the AIAA/SAE/ASME 17th Joint Propulsion Conference, July 1981.

20. Crump, J. E., K. C. Schadow, F. S. Blomshield, F. E. C. Culick, and V. Yang, "Combustion Instability in Dump Combustors: Acoustic Mode Determinations," *Proceedings of the 19th JANNAF Combustion Meeting, Greenbelt, Md., 4-7 October 1982*, Laurel, Maryland, Chemical Propulsion Information Agency (in process).

21. Naval Weapons Center, *Independent Research and Independent Exploratory Development Annual Report Fiscal Year 1981*, NWC TP 6328, China Lake, California, NWC (June 1982), 160 pp.

## Authors



James E. Crump, a research physicist at NWC since 1953, has done research on solid propellant combustion, in particular the combustion of aluminum in propellants, and on combustion instability. He has been involved with the development of a number of missile and solid propellant rocket motors and was the motor design engineer for an early version of the Sidewinder missile.



Klaus C. Schadow, a supervisory general engineer in the NWC Research Department, received his undergraduate education at the Technische Hochschule Hannover, Germany (FRG) and his Ph.D. from T H München, Germany (FRG). Since his arrival at NWC in 1970, his research has concentrated on airbreathing combustion-related problems.



H. Bernard Mathes, currently a supervisory research physicist, joined the NWC Research Department in 1956 and has been engaged primarily in measurement of dynamic phenomena, experimental acoustics, and combustion instability of solid propellant rocket motors. He has been involved with numerous missile and solid propellant rocket motor programs at NWC and is the holder or co-holder of two U.S. patents and three patent disclosures on acoustic and combustion devices.

# New Concepts for Thermal Batteries



by

M. H. Miles and A. N. Fletcher  
Naval Weapons Center

## Introduction

The first thermal batteries were developed by German scientists during World War II for several ordnance applications, including the V-1 and V-2 missiles.<sup>1</sup> Since then, thermal batteries have been widely used in military applications, including various missiles, proximity fuzes, shells, and atomic weaponry.<sup>2</sup> Maximum power from a thermal battery is needed for periods ranging from a few seconds to 60 minutes.

As electric power supplies for missile weapon systems, thermal batteries offer many advantages over alternate energy sources. These advantages include long shelf life (15-20 years), rapid and reliable activation, high discharge rates (100 mA/cm<sup>2</sup>), high power densities, and the ability to withstand high shock and spin forces.<sup>2</sup> Many of these advantages result from using inert salts that become a highly conductive electrolyte when the battery is activated by a pyrotechnic heat source that melts the salt.<sup>1,2</sup>

The major components of a thermal battery cell are illustrated in Figure 1. The anode (negative electrode) and cathode (positive electrode) in the galvanic cell are separated by a pad or pellet that contains the depolarizer, electrolyte salt, and binder. Thermal batteries remain inactive and inert as long as the salt mixture contained between the anode and cathode remains in its normal, nonconducting, inert, solid state. The sudden application of heat activates the battery by melting the salt, converting it into a liquid capable of conducting electrical charges (ions) between the anode and the cathode.

Most thermal batteries employed in weapon systems use a lithium chloride-potassium chloride (LiCl-KCl) salt mixture as the electrolyte layer. Calcium (Ca) metal is often selected as

the anode material, while calcium chromate (CaCrO<sub>4</sub>) generally serves as the active cathode material.<sup>1,3</sup>

The use of a LiCl-KCl salt mixture has several disadvantages. For instance, the melting point of the mixture limits the battery's activation to temperatures above 350° C. Furthermore, the Ca/LiCl-KCl/CaCrO<sub>4</sub> system exhibits complex side reactions that limit the operating temperature to between 500 and 600° C for satisfactory battery performance.<sup>3,4</sup> These high operating temperatures increase the quantity of pyrotechnic heating material and insulation required for cell activation and discharge. Another problem with LiCl-KCl batteries is that CaCrO<sub>4</sub>, the oxidizer (depolarizer) generally used, is a carcinogen.<sup>5,6</sup> The development of safety regulations regarding CaCrO<sub>4</sub> is likely to curtail its availability and endanger the production of thermal batteries that use it as an oxidizer. A promising new system uses molten lithium as the anode and iron disulfide (FeS<sub>2</sub>) as the oxidizer, i.e., Li/LiCl-KCl/FeS<sub>2</sub>.<sup>7,8</sup> This system is free of carcinogenic materials and is superior to the Ca/CaCrO<sub>4</sub> system in power and energy densities. Furthermore, this new thermal battery system does not have the performance-limiting side reactions characteristic of the Ca/CaCrO<sub>4</sub> battery chemistries.<sup>9</sup>

## Molten Nitrate Systems

The novel approach of using certain oxidizing molten salts, such as lithium nitrate (LiNO<sub>3</sub>), in thermal batteries has been developed at the Naval Weapons Center.<sup>10</sup> This approach is especially attractive because of the low melting points and nontoxic nature of these salts. Mixtures of LiNO<sub>3</sub>-potassium nitrate (KNO<sub>3</sub>) salts melt at temperatures as low as 124° C.

**Figure 1**

Major components of a simplified thermal battery cell.

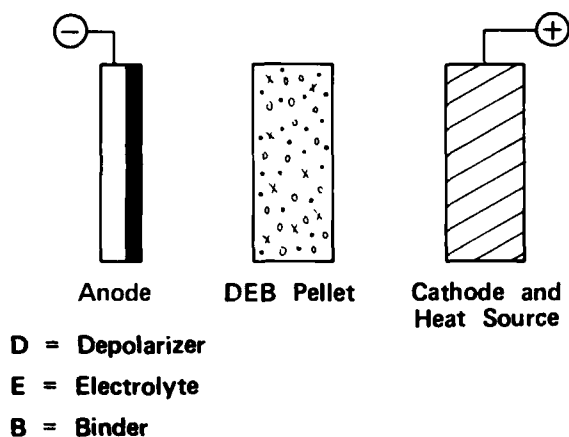
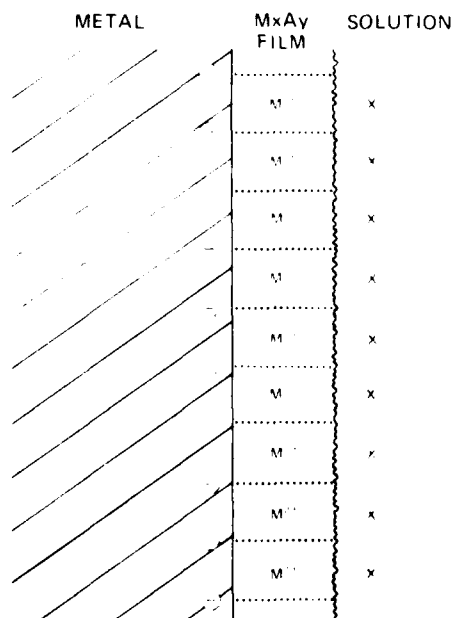


**Figure 2**

Schematic model for passivating films on metals. The term  $M_xA_y$  represents the nonstoichiometric film,  $M^{2+}$  represents the excess metal ions within the film, and  $X^-$  represents the anions electrostatically attracted to the film-solution interface. Actual films will not necessarily be uniform and may vary considerably in thickness.



Such a low melting temperature can shorten a battery's activation time and reduce the weight of heat sources and insulation. The  $\text{LiNO}_3$  salt may also function as the oxidizer, thus eliminating the need for  $\text{CaCrO}_4$ . The low operating temperatures also open the door to the use of various other oxidizers, binders, and anode materials that are not stable at higher temperatures.

#### Anode Reactions

Active metals, such as calcium, that are used as the thermal battery anode are not normally compatible with oxidizing molten salts such as  $\text{LiNO}_3$ . An inert protective film, however, limits the corrosive chemical reaction between the anode and the molten salt. Regulation of this passivating film is essential to good anode performance. If the passivating layer becomes too thick and hinders the passage of metal ions across the film and into the solution, the metal ions accumulate within the film and the battery performance deteriorates. For the calcium anode in molten  $\text{LiNO}_3$ , aggressive negative ions, such as chloride ions ( $\text{Cl}^-$ ), must be added to the molten nitrate to break up the passivating film sufficiently to allow the thermal battery cells to operate efficiently.<sup>11</sup>

A generalized model of the passivating film at the anode is shown in Figure 2. The excess metal ions ( $M^{2+}$ ) trapped within the film electrostatically attract negative ions ( $X^-$ ) to the film/solution interface. Passivating negative ions, such as nitrate ions ( $\text{NO}_3^-$ ), peroxide ions ( $\text{O}_2^{2-}$ ), or superoxide ions ( $\text{O}_2^-$ ), that contain oxygen atoms will repair breaks in a passivating oxide film. Aggressive negative ions, such as  $\text{Cl}^-$ , hinder the film repair action of the passivating ions through competitive adsorption at the film/solution interface.<sup>12</sup>

Theories on the corrosion of metals can readily be tested in molten salt electrolytes. Corrosion processes are much more rapid at the higher temperatures of these molten salt mixtures than they are at ordinary ambient conditions; thus, the important variables can be readily identified and studied. Despite the numerous studies of corrosion, there is no general recognition as yet of a specific theory or model that explains the passivity and corrosion of metals.<sup>13</sup> Generally recognized, however, is the concept that the presence of chloride ions causes pitting corrosion of metals that form stable oxide films. The model presented in Figure 2 is applicable to the passivity and corrosion of metals under a variety of conditions, including the passivity and film breakdown of active metal anodes used in thermal battery cells.<sup>12</sup>

The passivating film at the anode hinders the passage of metal ions into the solution; thus the excess of positive metal ions trapped within the film causes the open circuit potential of the anode to become more positive. With the breakdown of the passivating film, the excess metal ions escape and the potential of the anode shifts to more negative values. Figure 3 shows the breakdown by chloride ions of the passivating film on calcium anodes in several nitrate melts. Film breakdown was determined by the sudden change in the open circuit potential as measured against a silver ion-silver ( $\text{Ag}^+/\text{Ag}$ ) reference electrode. The effect of chloride ions on the calcium anode potential is much greater in molten  $\text{LiNO}_3$  than in either molten

sodium nitrate ( $\text{NaNO}_3$ ) or molten  $\text{KNO}_3$ . This difference is explained by considering the direct reaction of molten nitrates with calcium metal



to produce excess oxide ions ( $\text{O}^-$ ) in the melt. These oxide ions are innocuous in molten  $\text{LiNO}_3$  and simply precipitate as insoluble lithium oxide ( $\text{Li}_2\text{O}$ ). In molten  $\text{NaNO}_3$  and  $\text{KNO}_3$ , however, oxides are more soluble and form the more reactive ions  $\text{O}_2^-$  and  $\text{O}_2$ . Therefore, according to the model presented in Figure 2, the passivating  $\text{O}_2^-$  and  $\text{O}_2$  negative ions formed at the calcium surface in molten  $\text{NaNO}_3$  and  $\text{KNO}_3$  block the desired aggressive action of the added  $\text{Cl}^-$  ions. As a result, smaller shifts are observed in the open circuit potential of the calcium anode.<sup>12</sup> The results favor the use of  $\text{LiNO}_3$  rather than  $\text{NaNO}_3$  or  $\text{KNO}_3$  in thermal battery cells using calcium anodes.

New directions for research on the anode component of thermal battery cells are suggested by the passivating film model in Figure 2. The nature of the passivating film as well as the rate of transport of metal ions across the film would be likely to vary greatly from one active metal to another. These considerations suggest the study of other active metal anodes, such as lithium magnesium, strontium, scandium, and yttrium, in molten nitrates. Because of its much smaller size, the lithium ion ( $\text{Li}^+$ ) has a faster transport rate across the passivating film than do larger metal ions such as  $\text{Ca}^{++}$ . The low melting point of lithium metal ( $188^\circ\text{C}$ ), however, requires that this metal be used in the form of higher melting compounds or alloys. Preliminary studies have shown that the use of lithium composites as anodes in molten nitrates yields high current densities with very little polarization.

### Cathode Reactions

The second major component of a thermal battery cell is the cathode. Oxidizing molten salts such as nitrates can function both as the electrolyte and the active cathode material. The performance of the molten nitrate cathode is determined principally by the nature of the positive metal ions present. Experimentally, the potential of the  $\text{LiNO}_3$  cathode is about a full volt better than that of the  $\text{KNO}_3$  cathode.<sup>14</sup> The performance of the molten nitrate cathode varies inversely with the metal ion radius and decreases in the order  $\text{LiNO}_3 > \text{NaNO}_3 > \text{KNO}_3$ . A model for the electrochemical reduction of molten nitrates is presented in Figure 4. The stronger positive electric field surrounding the smaller metal ion aids both the slow transfer of the electron from the electrode to the nitrate ion, and the rupture of the N-O bond.<sup>14,15</sup>

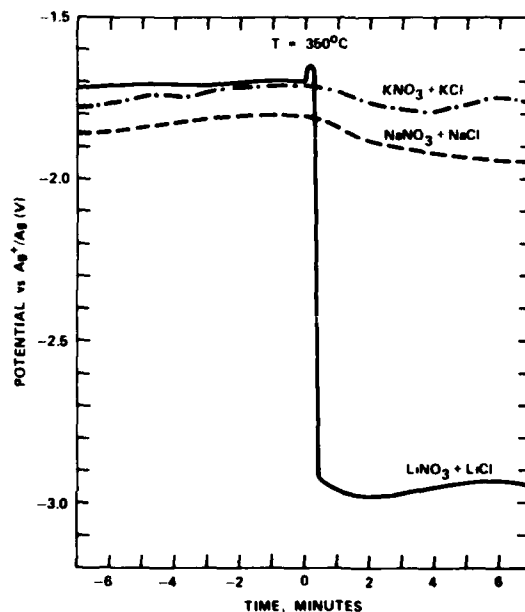
The cathodic reaction in molten  $\text{LiNO}_3$  cells



produces insoluble  $\text{Li}_2\text{O}$  as a product. Severe cell polarization occurs when  $\text{Li}_2\text{O}$  is formed at the electrode surface faster than it can be removed, thus blocking the reacting  $\text{LiNO}_3$  from reaching the electrode surface and slowing the rate of the cathodic reaction. The polarization of the cathode becomes the limiting factor in obtaining useful cell voltages at current densities above  $50 \text{ mA/cm}^2$ .

**Figure 3**

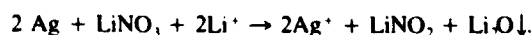
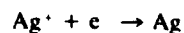
Effects of addition of 10-mole-percent chloride salts on the open-circuit potentials of the calcium anode in molten  $\text{KNO}_3$ ,  $\text{NaNO}_3$ , and  $\text{LiNO}_3$  at  $350^\circ\text{C}$ . Chloride additions were made at time zero.



### Cathode Performance Improvement

Adding small amounts of silver nitrate ( $\text{AgNO}_3$ ) to molten nitrates greatly improves the performance of the cathode.<sup>16</sup> Figure 5 shows that adding 0.1-mole-percent  $\text{AgNO}_3$  to molten  $\text{LiNO}_3$  at  $350^\circ\text{C}$  permits the cathode to sustain a current density of  $100 \text{ mA/cm}^2$  without the onset of the severe passivation observed in pure  $\text{LiNO}_3$ . The deposition of silver particles on the electrode surface increases its effective area, thereby minimizing the blocking action caused by the insoluble  $\text{Li}_2\text{O}$  formed. In the presence of 1.0-mole-percent  $\text{AgNO}_3$ , the direct reduction of silver ions ( $\text{Ag}^+$ ) yields stable potentials close to that of the  $\text{Ag}^+/\text{Ag}$  reference electrode (Figure 5).<sup>2</sup>

Long-term discharge experiments indicate that a recycling of silver ions takes place by reactions such as



This corrosive oxidation of the deposited silver metal by the molten  $\text{LiNO}_3$  recycles the  $\text{Ag}^+$  ions. This reaction, like many others in molten nitrates, depends on the nature of the positive

**Figure 4**

Postulated reaction steps for the electrochemical reduction of molten nitrates showing the involvements of the positive metal ion.

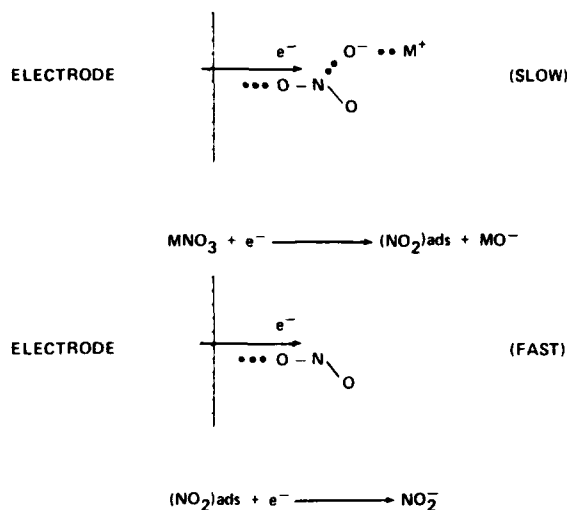
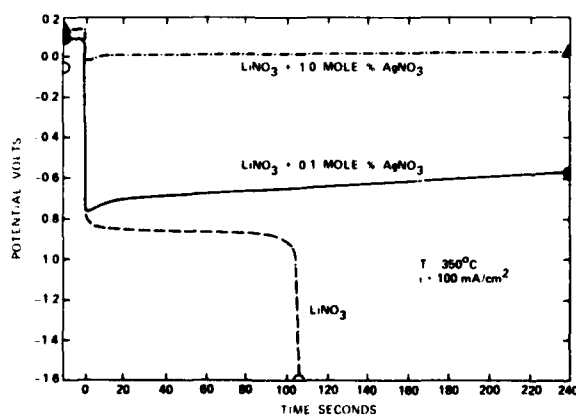


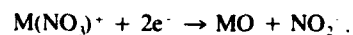
**Figure 5**

Effect of silver nitrate addition on the performance of the cathode during constant current studies at 100 mA/cm<sup>2</sup> in molten LiNO<sub>3</sub> at 350° C.



metal ion present and is much slower in molten NaNO<sub>3</sub> or KNO<sub>3</sub> than in molten LiNO<sub>3</sub>.

Various other metal ion additives have also been tested in molten nitrates. Of those tested, only lead (Pb<sup>++</sup>) and cadmium (Cd<sup>++</sup>) ions showed any evidence for a cathodic reaction; however, in contrast to the reaction of silver ions, there is no evidence for a new metallic phase ever forming on the electrode surface. Naval Weapons Center studies suggest that reduction to the free metal never occurs for Pb<sup>++</sup> or Cd<sup>++</sup> ions in molten nitrates; instead the NO<sub>3</sub><sup>-</sup> ion in Pb(NO<sub>3</sub>)<sup>+</sup> or Cd(NO<sub>3</sub>)<sup>+</sup> complexes is the actual substance reduced; i.e.,



Unlike the cathodic reaction of silver ions, electrons rather than metal ions transfer the charge across the electrode/molten nitrate interface. The strong electric field of the divalent Pb<sup>++</sup> or Cd<sup>++</sup> ion in these complexes lowers the free energy of activation for the reduction of the nitrate ion. Thus a new reduction wave at a more positive potential is observed. These studies substantiate the major role of the metal ion on the electrode reduction of molten nitrates (Figure 4).

## Cell Discharge

Results of the separate fundamental studies of the anode and cathode in molten nitrates can be used to design thermal battery cells that yield the optimum performance.<sup>17</sup> A thermal battery system using these results is represented by the cell



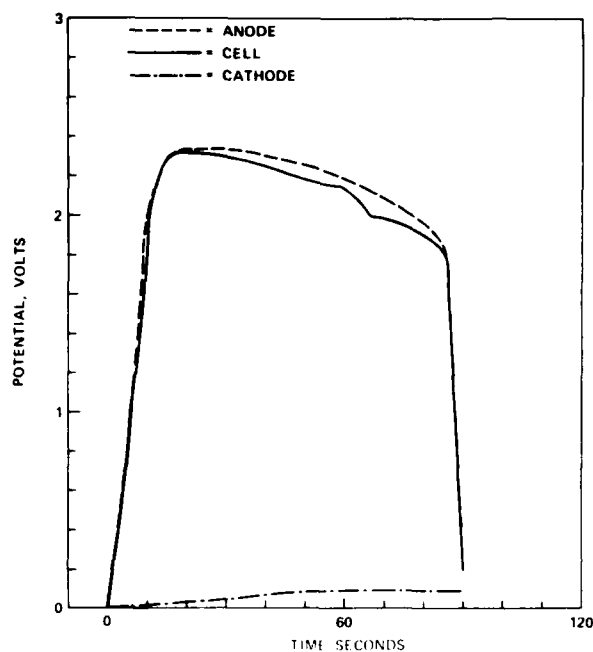
with the LiNO<sub>3</sub> incorporated into a fiberglass binder, LiCl layered near the anode, and AgNO<sub>3</sub> layered near the cathode. The fiberglass binder also acts as a separator and confines the LiCl and AgNO<sub>3</sub> additives to the anode and cathode regions, respectively, where they are most effective. A typical discharge of this cell is shown in Figure 6. At a discharge rate of 75 mA/cm<sup>2</sup>, the cell potential remains above 2 volts for over 60 seconds. This cell was designed to supply a high current density for a short time. Other thermal battery cells that use molten nitrates can be designed with different properties, such as discharge times exceeding 60 minutes at 10 mA/cm<sup>2</sup>.<sup>12,16</sup>

## References

1. Van Domelen, B.H., and R. D. Wehrle, "A Review of Thermal Battery Technology", *Ninth Intersociety Energy Conversion Engineering Conference Proceedings*, New York, American Society of Mechanical Engineers (1974) pp. 665-670.
2. DeMarco, F., K. Heitmann, and K. Press, "Thermal Batteries—Unique Power Supplies," *Advanced Battery Technology*, 16 (February-March 1980) p. 81.
3. Nissen, D. A., "A Study of the Anode-Electrolyte Interface in a Thermal Battery," *Journal of the Electrochemical Society*, 126 (1979) p. 176.

**Figure 6**

Discharge of a  $\text{Ca/LiCl, LiNO}_3/\text{LiNO}_3, \text{AgNO}_3/\text{Ni}$  cell at  $375^\circ\text{C}$  using a constant current density of  $75 \text{ mA/cm}^2$ . Cell diameter was 1.3 centimeters



4. Bush, D. M., "Results of Thermal Battery Cell Testing," *Proceedings of the Twenty-Sixth Power Sources Symposium*, Red Bank, New Jersey, PSC Publications Committee (1974) pp. 144-147.

5. Bishop, W. S., and A. A. Benderly, "Critical Materials in Thermal Batteries," *Proceedings of the Twenty-Seventh Power Sources Symposium*, Red Bank, New Jersey, PSC Publications Committee (1978) pp. 158-160.

6. "OSHA Issues Tentative Carcinogen List," *Chemical Engineering News* 56 (July 31, 1978) pp. 20-22.

7. Fraser, R. T. M., L. J. Pearce, and D. C. P. Birt, "High Rate Lithium-Iron Disulfide Batteries," *Proceedings of the Twenty-Ninth Power Sources Conference*, Pennington, New Jersey, The Electrochemical Society (1980) pp. 43-45.

8. Winchester, C. S., "The LAN- $\text{FeS}_2$  Thermal Battery System," *Proceedings of the Thirtieth Power Sources Conference*, Pennington, New Jersey, The Electrochemical Society (in press).

9. Trepper, F., and L. Daniel, "Advanced Thermal Batteries," *Minutes, Chemical Working Group, Interagency Advanced Power Group*, Philadelphia, Pennsylvania, Franklin Research Center (19 November 1982) pp. J, 1-58.

10. Miles, M. H., and A. N. Fletcher, "Thermal Battery Cells Utilizing Molten Nitrates as the Electrolyte and Oxidizer," *Journal of Applied Electrochemistry*, 10 (1980), p. 251.

11. Miles, M. H., D. A. Fine, and A. N. Fletcher, "The Calcium Anode in Molten Nitrate Electrolytes," *Journal of the Electrochemical Society*, 125 (1978) p. 1209.

12. Miles, M. H., "The Breakdown of Passive Films on Active Metal Anodes by Halide Ions in Oxidizing Molten Salts," *Journal of Applied Electrochemistry*, 11 (1981) p. 325.

13. Frankenthal, R. P., and J. Kruger, Editors, *Passivity of Metals*, The Electrochemical Society, Princeton, New Jersey, (1980).

14. Miles, M. H., and A. N. Fletcher, "Cation Effects on the Electrode Reduction of Molten Nitrates," *Journal of the Electrochemical Society*, 127 (1980) p. 1761.

15. Fletcher, A. N., M. H. Miles, and M. L. Chan, "The Effect of Temperature on the Cathodic Behavior of Some Fused Nitrate Salts," *Journal of the Electrochemical Society*, 126 (1979) p. 1496.

16. Miles, M. H., and A. N. Fletcher, "High Rate Discharge of  $\text{Ca/LiClO}_4\text{-LiNO}_3$  Thermal Battery Cells," *Journal of the Electrochemical Society* 128 (1981) p. 1489.

17. McManis, G. E., M. H. Miles, and A. N. Fletcher, "High Power Density Thermal Battery Technology Utilizing Oxidizing Molten Salts," *Thirtieth Power Sources Symposium Proceedings* (1982) (in press).

## Authors

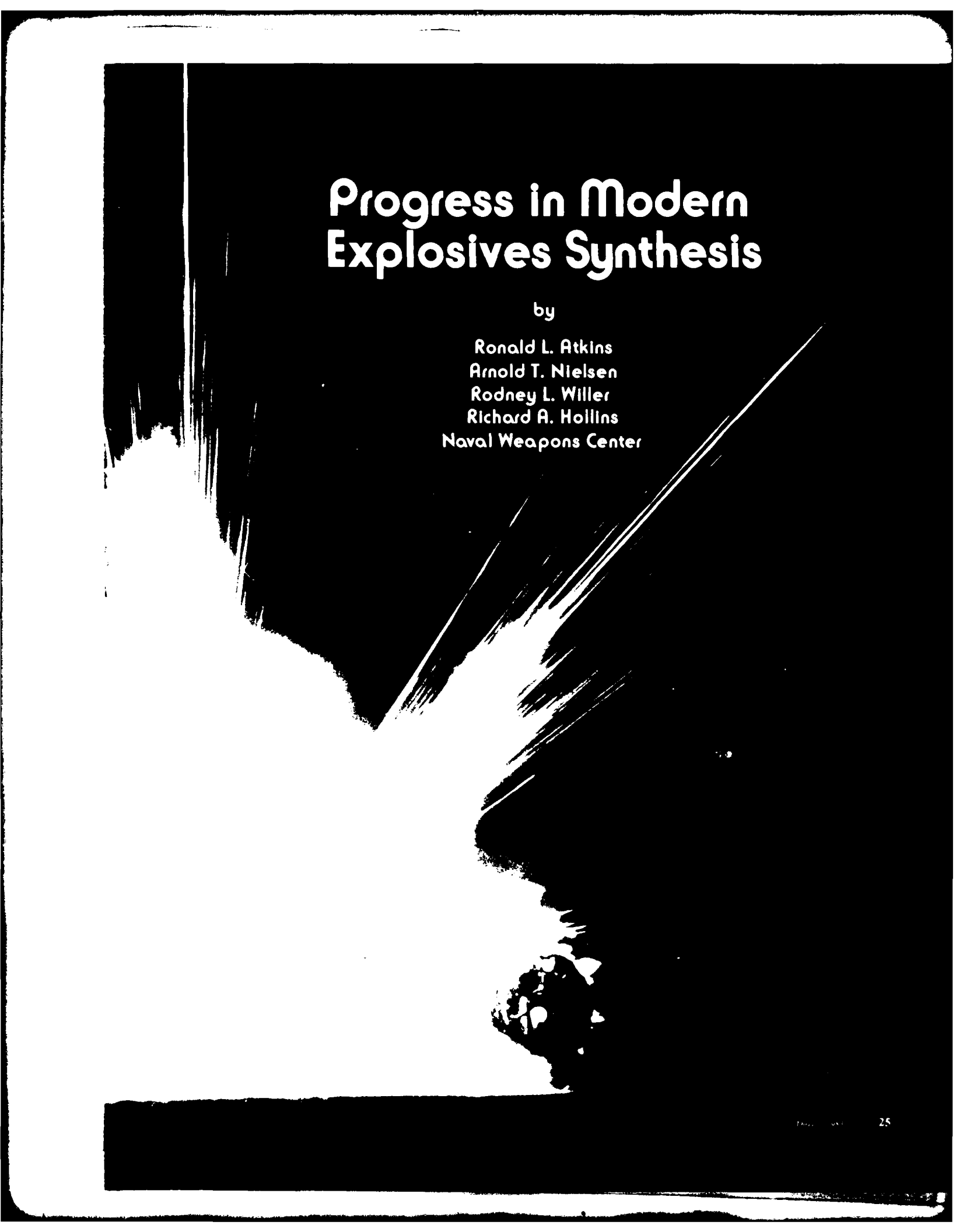


Melvin H. Miles is a research chemist at the Naval Weapons Center. Before coming to the Center in 1978, he was an associate professor at Middle Tennessee State University. His major research interests are the kinetics and mechanisms of electrode reactions. He received a B.A. degree in chemistry from Brigham Young University in 1962 and a Ph.D. from the University of Utah in 1966. He was awarded a NATO postdoctoral fellowship and did research in electrochemistry with Dr. Heinz Gerischer in Germany. Dr. Miles has authored more than 55 technical papers.



Aaron N. Fletcher has been a research chemist at the Naval Weapons Center since 1954 and is presently head of the Energy Chemistry Branch. His research interests are batteries, electrochemical synthesis, dyes for laser applications, and fluorescence spectroscopy. He received a B.S. degree from the California Institute of Technology in 1949 and a Ph.D. in analytical chemistry from the University of California at Los Angeles in 1961. Dr. Fletcher was awarded two 1-year educational fellowships beginning in 1959.





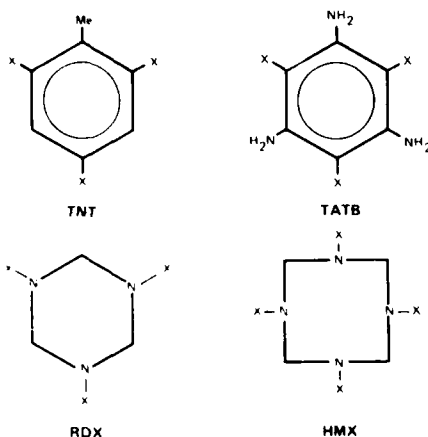
# Progress in Modern Explosives Synthesis

by

Ronald L. Atkins  
Arnold T. Nielsen  
Rodney L. Willer  
Richard A. Hollins  
Naval Weapons Center

**Figure 1**

Modern military explosives.



X = NO<sub>2</sub>

## Introduction

The next generation of naval ordnance now in the planning, research, and development cycle requires new energetic materials to fulfill new ordnance performance and survivability requirements. To meet these requirements, the Naval Weapons Center supports an active, multifaceted, in-house research effort in energetic materials synthesis and evaluation. Programs range from research projects of theoretical interest in the design and synthesis of new explosive molecules, to applied projects on formulation and evaluation of new explosive and propellant systems. The program is guided by the requirements defined by the systems design engineers and includes new high-density high-energy explosives for volume-limited systems and insensitive high explosives for applications that call for new explosives that are insensitive to shock and extreme temperatures. All new systems need to minimize hazards associated with manufacturing, processing, loading, deployment, and demilitarization. The research goal at NWC is to combine these diverse needs and develop the new generation of energetic materials required by future weapon systems.

## Modern Military Explosives

Most modern military explosives are composed of a binder material, a solid crystalline explosive compound, and various additives. The binder, generally a polymer, has two functions: it holds the composite mixture together, and it imparts mechanical properties to the mixture. Additives are used to adjust the chemical, physical, and explosive properties of the resultant explosive formulation. The solid crystalline explosive compounds most often used in high-performance explosive formulations are 2,4,6-trinitrotoluene (TNT), 1,3,5-trinitro-1,3,5-triazacyclohexane (RDX), 1,3,5,7-tetraazacyclooctane (HMX), and 1,3,5-triamino-2,4,6-trinitrobenzene (TATB). (See Figure 1 for the chemical compositions of these compounds and Table 1 for the physical, chemical, and explosive properties of these compounds.)

**Table 1**

Physical, Chemical, and Explosive Properties of TNT, TATB, RDX, and HMX

Compound	Density (g/cc)	Melting point (°C)	Detonation velocity (m/s)	Detonation pressure (kbar)	Impact sensitivity (H <sub>50</sub> cm)
TNT	1.65	81	6,930	210	75
TATB	1.94	325	7,760	291	350 <sup>a</sup>
RDX	1.81	205	8,700	338	28
HMX	1.90	285	9,110	390	20

<sup>a</sup> Estimated

If the next generation of energetic materials is to be useful, the materials should have the density and energy of RDX and HMX and the reduced sensitivity to an inadvertent initiation of TNT and TATB. These extreme requirements may be mutually exclusive, but reasonable tradeoffs of performance and hazard properties can and must be made to develop the required materials. Research is providing new methodology and new materials for future use in energetic materials applications, which include polynitroaromatic, insensitive, and new polynitramine explosives.

### Polynitroaromatic Explosives

Hexanitrobenzene (HNB) belongs to a class of zero hydrogen explosives called nitrocarbons and is composed only of nitro groups attached to carbon ( $C_6(NO_2)_6$ ). After a more than 40-year effort by free world scientists, NWC research chemists succeeded in 1978 in synthesizing HNB from pentanitroaniline (PNA) as shown in Figure 2.<sup>1</sup> HNB is the most energetic organic explosive known. The key to the HNB synthesis was the development of a new, generally applicable procedure for the oxidation of weakly basic amines to nitro functionality. This new procedure uses *in situ* generated peroxydisulfuric acid as the oxidant. HNB was only the third nitrocarbon explosive reported in the literature. The synthesis procedure was used to prepare many new polynitro-substituted explosives and was recently adapted for the preparation of a new zero hydrogen explosive, decanitrobiphenyl (DNBP) as shown in Figure 3.<sup>2</sup> DNBP joins the select list of zero hydrogen nitrocarbon explosives, along with HNB, tetranitromethane (TNM), and hexanitroethane (HNE).<sup>4,5</sup> DNBP was prepared from 4,4'-diamino-2,2',3,3',5,5',6,6'-octanitrobiphenyl (ONBP) by oxidation with peroxydisulfuric acid. DNBP is chemically similar to but more reactive than HNB. Present observations suggest that the thermal stabilities of the known nitrocarbons decrease in the order of tetranitromethane > hexanitroethane > hexanitrobenzene > decanitrobiphenyl. Research efforts are continuing in this area of explosives synthesis.

### Insensitive High Explosives

Energetic materials research at NWC also involves the synthesis of new insensitive high explosives having both explosive properties equal to or greater than RDX or HMX and sensitivity properties similar to those of TATB in resistance to thermal, shock, and impact initiation. The amino group has been identified as a mediator of explosive sensitivity. It also serves as an activating group for electrophilic aromatic substitution reactions. The presence of an amino group on the aromatic nucleus thus serves a dual purpose of allowing the simultaneous introduction of nitro groups in the aromatic nucleus and imparting the desired sensitivity properties. This dual nature is illustrated by the synthesis of DNBP as shown in Figure 3. ONBP is prepared by nitration of the tetranitro precursor, 4,4'-diamino-2,2',6,6'-tetranitrobiphenyl (TNBP).

**Figure 2**

Synthesis of HNB.

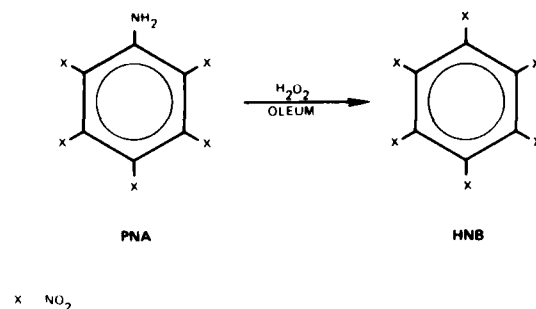
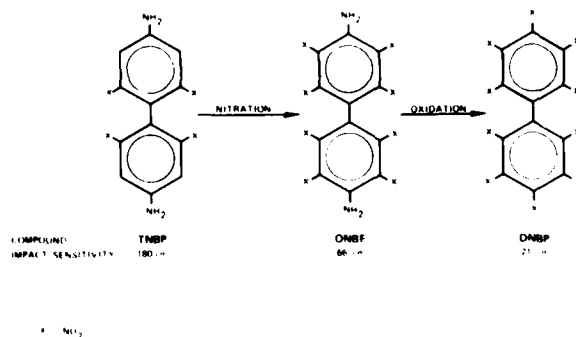


**Figure 3**

Synthesis of decanitrobiphenyl.



This nitration would not proceed without the activation and directive influence of the 4,4' amino groups. Oxidation of ONBP amino groups is accomplished using peroxydisulfuric acid. Comparison of the ONBP versus the DNBP impact sensitivities shows the sensitivity mediation effects of the 4,4' amino substituents.

The amino group with its dual nature was used advantageously to prepare a large number of previously inaccessible aromatic explosives. TNT has served as a very convenient precursor to these new explosives. TNT, which is available in vast quantities at low cost, can be selectively reduced to yield two isomeric dinitrotoluidines. Ammonium hydroxide catalyzed reduction of TNT by H<sub>2</sub>S in dioxane solvent results in para-nitro group reduction giving 4-amino-2,6-dinitrotoluene (*p*-DNT). The ortho isomer, 2-amino-4,6-dinitrotoluene (*o*-DNT), is obtained by reduction of TNT with iron metal in acetic acid. The remaining meta isomer (*m*-DNT) could not be obtained directly from TNT, but was obtained from meta toluic acid (MTA) in several steps. The three dinitrotoluidines can be readily nitrated in mixed acid to give the desired tetranitrotoluidines as summarized in Figure 4. The three isomeric tetranitrotoluidines have better calculated explosive properties than TNT. The densities are

slightly higher than TNT but less than expected when calculated by the Holden method (1.76 g/cc).<sup>6</sup> The tetranitrotoluidines are slightly more sensitive to impact than TNT, but considerably less sensitive than RDX or HMX as shown in Table 2.

**Table 2.**

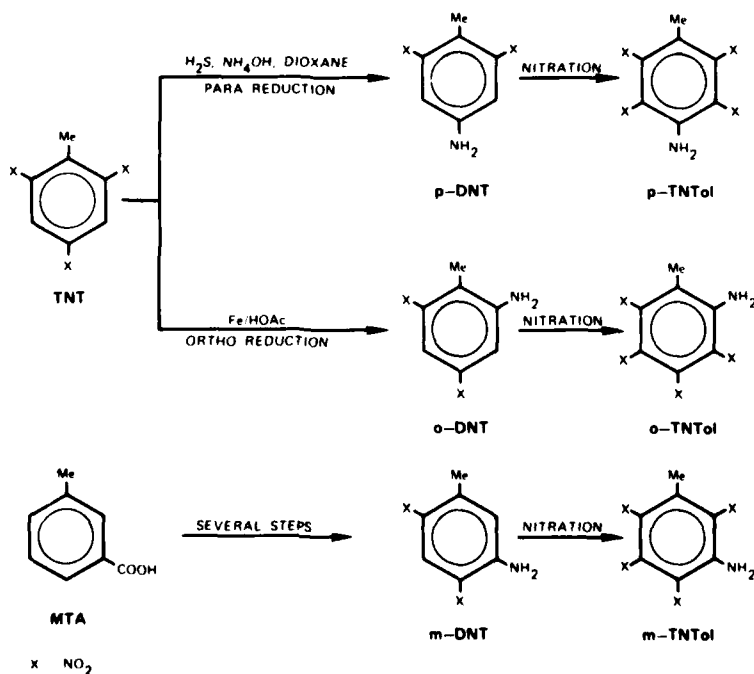
*Comparative Properties of Tetranitrotoluidines.*

Compound	Density (g cc)	Detonation velocity (m. s)	Detonation pressure (kbar)	Impact sensitivity (H <sub>50</sub> cm)
TNT	1.65	6,900	210	70
Ortho	1.72	7,700 <sup>a</sup>	269 <sup>a</sup>	36
Meta	1.73	7,700 <sup>a</sup>	269 <sup>a</sup>	37
Para	1.72	7,700 <sup>a</sup>	269 <sup>a</sup>	47
HMX	1.90	9,100	390	25

<sup>a</sup> Calculated.<sup>7</sup>

**Figure 4**

*Synthesis of the isomeric tetranitrotoluidines.*



The three isomeric tetranitrotoluidines can be used as effective precursors of other explosives. Oxidation using peroxydisulfuric acid gives pentanitrotoluene (PNT) in high yields. The overall conversion of TNT to PNT is 80% when prepared from para-tetranitrotoluidine, making this excellent explosive readily available. PNT has a measured density of 1.76 g/cc (calculated = 1.82 g/cc), has very good calculated explosive properties (detonation velocity = 8,200 m/s, detonation pressure = 312 kbar), and exhibits sensitivity similar to RDX (22 cm versus 25 cm).

When the mixed acid nitrations of the dinitrotoluidines are carried out at reduced temperatures and/or acid strength, pernitrate intermediates can be isolated, as shown in Figure 5, for the para isomer. These nitramine intermediates are thermally unstable and slowly evolve nitrogen oxides if allowed to stand at room temperature. However, if the nitramine is suspended in concentrated sulfuric acid and then treated with anisole, the nitramine is cleaved, giving high yields of the corresponding tetranitrotoluidine. Attempts to purify these intermediate nitramines by recrystallization led to the discovery that they undergo facile thermal rearrangement to yield benzenediazooxides as shown in Figure 5 for PNTol. This facile nitramine rearrangement is characteristic for polynitro aromatic nitramines and has made possible the preparation of many new extremely sensitive and powerful polynitrobenzenediazooxides. (Diazooxides are known as primary explosives: DINOL, 4,6-dinitrobenzene-2-diazo-1-oxide was used as a primary.) These new explosives may be useful as lead azide replacements in new ordnance.

Para-tetranitrotoluidine has been found to undergo unique chemistry in its own right. When the mixed acid nitration of the precursor dinitrotoluidine (p-DNT) is carried out at elevated temperatures, a remarkable transformation occurs—not only is the ring pernitrate, but the methyl substituent is also removed and replaced by a fifth nitro group to give 50 to 55% yield of pentanitroaniline as shown in Figure 6. This unexpected transformation involves oxidative demethylation of the aromatic ring followed by normal mixed acid nitration of the vacated para position. The importance of this discovery is that PNA serves as a convenient precursor to two very important explosives: HNB and TATB. Oxidation of PNA with peroxydisulfuric acid gives high yields of HNB. If PNA is dissolved in methylene chloride and then treated with ammonia, high yields of TATB are obtained. Readily available TNT becomes a precursor not only for the most powerful organic explosive yet synthesized (HNB) but also to the archetypal insensitive high explosive TATB. The rich chemistry of TNT is shown in Figure 7.

### Synthesis of Nitramine Explosives

As noted, earlier, the cyclic aliphatic nitramine explosives, RDX and HMX, are the most energetic materials now used in high-performance high-energy applications of naval ordnance and propellant systems. The performance of new explosives is measured against these benchmark materials.

**Figure 5**

Nitramine rearrangement to diazooxide and cleavage by anisole to the free amine.

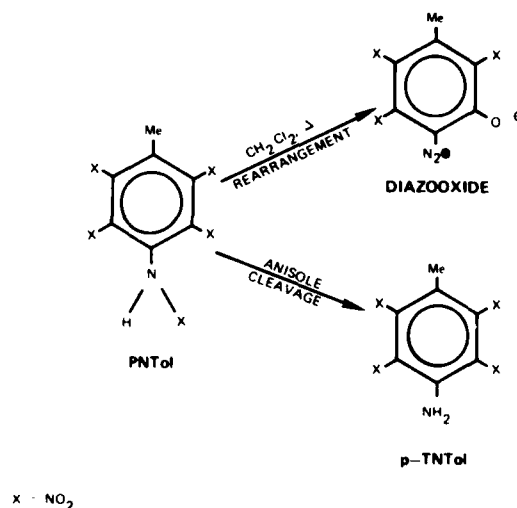


**Figure 6**

Conversion of p-DNT to PNA.

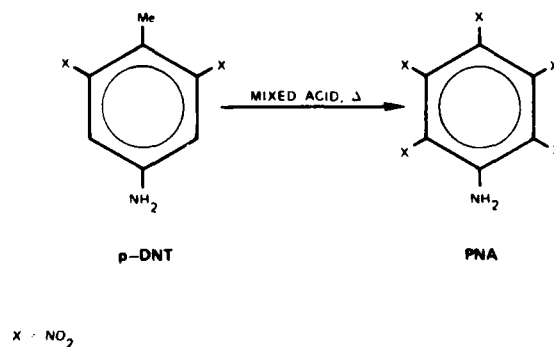
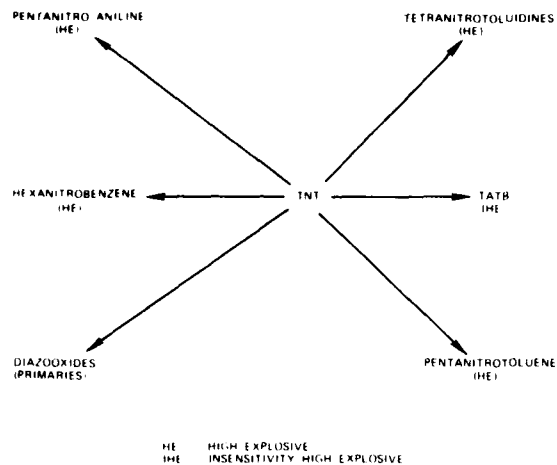


**Figure 7**

Explosives derived from TNT. HE is high explosive and IHE is insensitive high explosive.



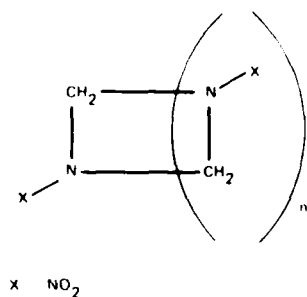
Empirical calculations, practice, and experience indicate that RDX and HMX are not at the limit of energy content achievable from this class of high-explosive compounds. Calculations show that increasing ring size in these compounds may lead to increased density.<sup>8</sup> RDX and HMX can be considered the second and third members of a homologous series of nitramine explosives. Other members of this series are unknown but in principle can be prepared simply by adding an additional methylene-nitramine unit to the ring skeleton as shown in Figure 8.

Constraining the molecular structure further by additional bridging to yield polycyclic molecules also may induce increased energy, density, and stability. (Density will increase in the structural alteration: acyclic < monocyclic < bicyclic < polycyclic < condensed polycyclic (caged) molecule.) Typical molecules of this type are shown in Figure 9 and are representative of the target compounds of the nitramine explosive synthesis program now being carried out at NWC.

The synthesis of macrocyclic and polycyclic nitramine explosives depends on the development of new synthetic techniques and methodologies. Recent work has concentrated on developing this new technology and applying it to the synthesis of new nitramine explosives. A new method for the

**Figure 8**

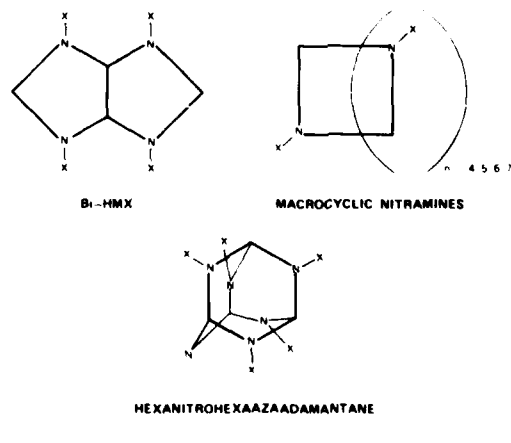
Macrocyclic nitramine explosives.



n	RING SIZE	COMPOUND	DENSITY	
			CALCULATED	MEASURED
1	4	UNKNOWN	1.72	—
2	6	RDX	1.91	1.81
3	8	HMX	2.01	1.91
4	10	UNKNOWN	2.07	—
5	12	UNKNOWN	2.09	—
6	14	UNKNOWN	2.09	—

**Figure 9**

Cyclic nitramine explosive target molecules.



synthesis of 1,3-dinitro-1,3-diazacycloalkanes was developed.<sup>9</sup> The discovery that alpha omega diamines can be trapped *in situ* with formaldehyde to form the corresponding dinitroso compound, when treated with nitrous acid, was pivotal. Nitrolysis of the dinitroso intermediates proceed in high yield to give the corresponding nitramine, when reacted with 100% nitric acid as shown in Figure 10. Reaction of an alpha omega diamine with formaldehyde generates a 1,3-diazacycloalkane (aminal). The aminal is trapped *in situ* by adding nitrous acid yielding a 1,3-dinitroso-1,3-diazacycloalkane. Nitrolysis proceeds with excellent yields using 100% nitric acid to give the desired nitramine. This technique has been applied to the synthesis of several interesting polycyclic polynitramine compounds such as 2,4,6,8-tetranitro-2,4,6,8-tetranitrospiro[5.5]undecane (TNSU). TNSU was prepared from tetrakis(aminomethyl)methane (TAM) as shown in Figure 11. TNSU is more energetic than TNT yet has approximately the same impact sensitivity (65 cm).

Members of the decalin family of tetraazanitramines were prepared using similar methodology: *trans*-1,3,5,7-tetranitro-1,3,5,7-tetraazadecalin was prepared from 1,2,3,4-tetraamino butane, which was derived in several steps from

**Figure 10**

Synthesis of 1,3-dinitro-1,3-diazacycloalkanes.

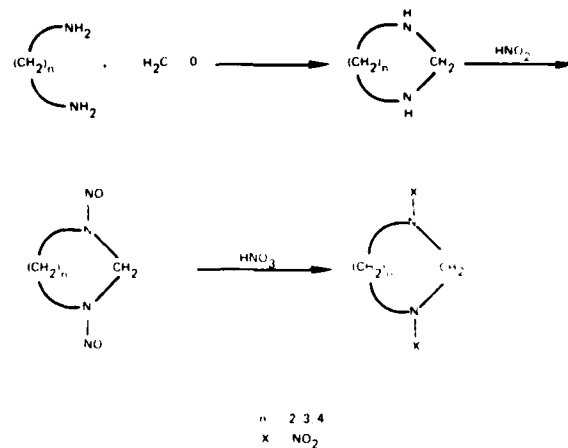


**Figure 11**

Synthesis of TNSU.

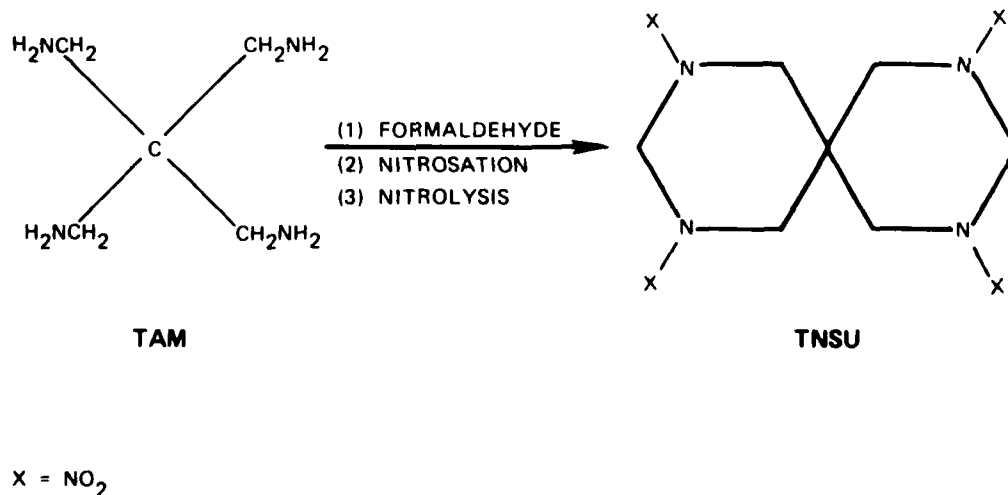


**Figure 12**

Synthesis of *cis*- and *trans*-1,3,5,7-tetranitro-1,3,5,7-tetragadecalin.

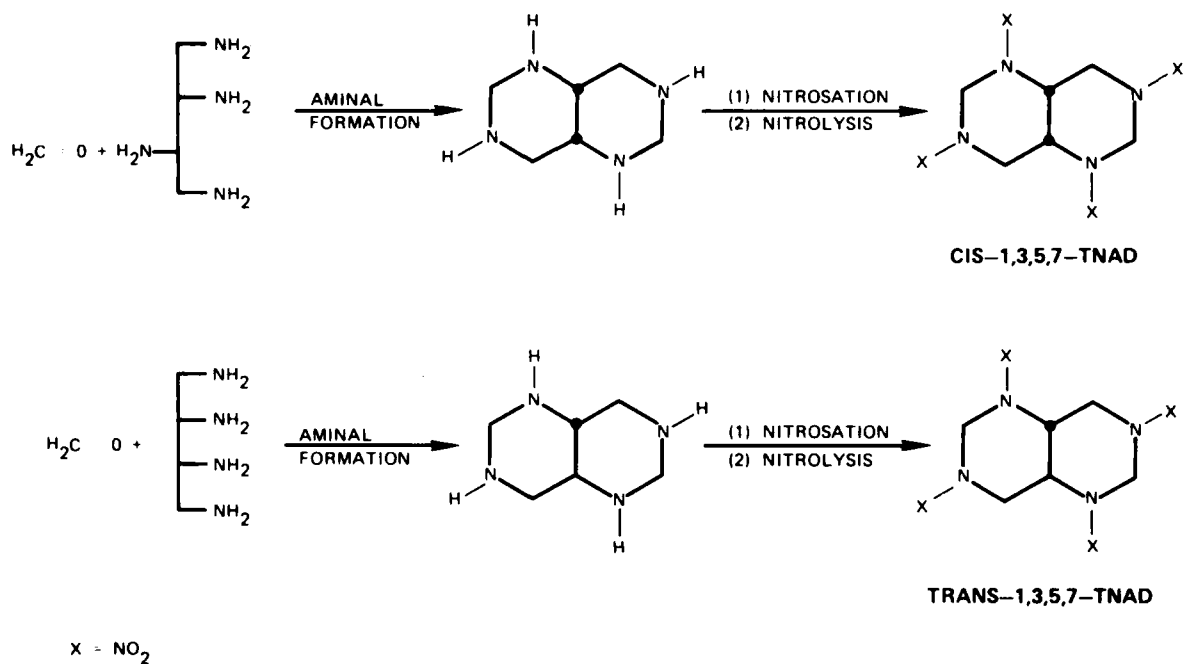
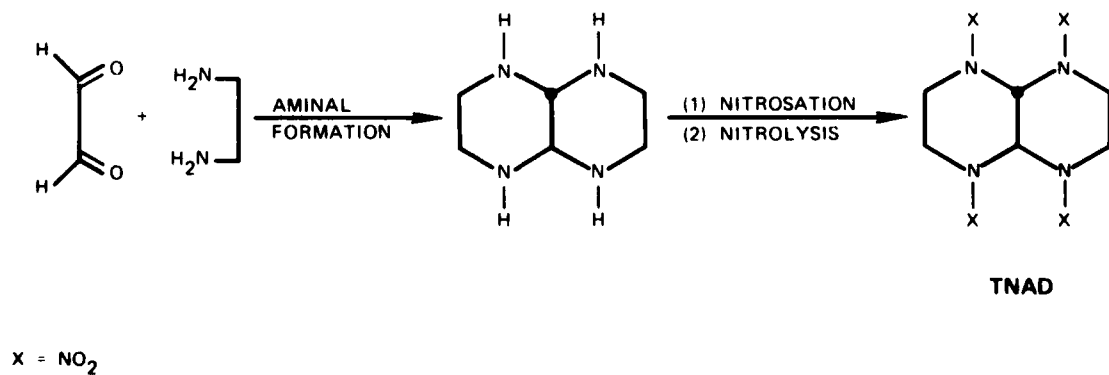


**Figure 13**

Synthesis of TNAD.



diethyltartrate. The isomeric *cis*-1,3,5,7-tetranitro-1,3,5,7-tetraazadecalin was prepared in a similar manner (see Figure 12).<sup>10</sup>

Substitution of glyoxal for formaldehyde, which is an adaptation of this new procedure, was used to prepare another member of this family of energetic materials, *trans*-1,4,5,8-tetranitro-1,4,5,8-tetraazadecalin.<sup>11</sup> This material was prepared by condensation of glyoxal with ethylene diamine followed by nitrosation to give the tetranitroso derivative. Nitrolysis of the nitroso substituents was accomplished using 100% nitric acid as shown in Figure 13. The three decalins are all well-behaved solids with good thermal stability. Their physical and explosive properties are listed in Table 3.

**Table 3.**

*Properties of the Tetranitrotetraazadecalin Series.*

Compound	Melting point (°C)	Density (g/cc)	Detonation velocity <sup>a</sup> (m/s)	Impact sensitivity (H <sub>50</sub> cm)
Trans-2,4,5,8	234	1.80	8.21	40
Cis-1,3,5,7	238	1.78	8.21	...
Trans-1,3,5,7	252	1.75	8.21	...

<sup>a</sup> Calculated.

The methodology described above has been used to prepare a new explosive compound with properties that exceed those of RDX and HMX. The synthetic strategy employed required the replacement of ethylene diamine with a suitable energetic 1,2-diamine, 4,5-diaminofurazan (DAF) for the condensation reaction with glyoxal. Modified literature methods were used for the diamine preparation.<sup>12,13,14</sup> As shown in Figure 14, when the diamine is condensed with glyoxal, a good yield of the desired bis-furazanodecalin (BFD) parent compound is obtained. The nitration of the tetramine by nitric acid in trifluoroacetic acid (TFA) proceeds as expected, and CL-15 (1,4,5,8-tetranitro-1,4,5,8-tetraazadifurazano (3,4-c)(3,4-h)decalin) is prepared in good yield.<sup>15</sup> A comparison of the properties for CL-15 and HMX is shown in Table 4.

**Table 4.**

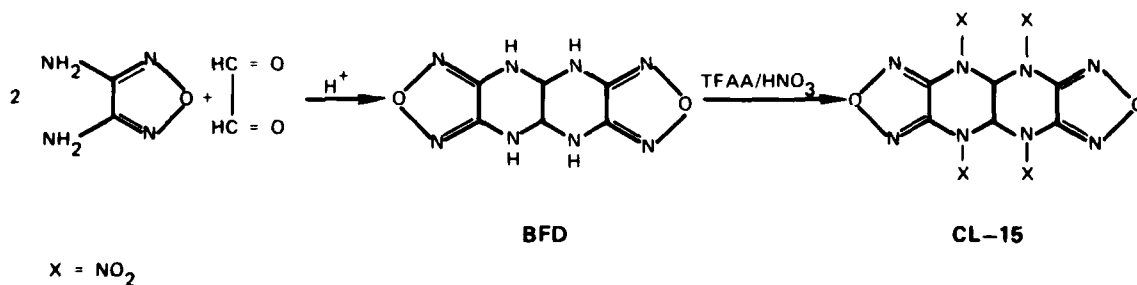
*Properties of CL-15 and HMX.*

Compound	Density (g/cc)	Detonation velocity (m/s)	Detonation pressure (kbar)
CL-15	1.98	9.57 <sup>a</sup>	437 <sup>a</sup>
HMX	1.90	9.05	393

<sup>a</sup> Calculated.<sup>16</sup>

**Figure 14**

*Synthesis of CL-15.*



In the early studies of CL-15 the compound was noted to be thermally unstable. Samples of the compound left at room temperature soon evolved red gas; samples left for prolonged time periods decomposed to intractable material. The heat of formation of CL-15 is +185 kcal/mole as determined by the standard back calculation technique from the heat of combustion. Using the heat of formation and the measured density, the performance parameters were calculated by the Kamlet method.<sup>16</sup> CL-15 exceeds HMX in explosive performance. While CL-15 does not have the required thermal properties, its successful synthesis demonstrates the possibility of exceeding HMX performance. Preparation is expected of other explosives having this energy content and the requisite stability properties.

### Acknowledgements

The authors wish to recognize Dr. W. P. Norris, Dr. R. A. Henry, T. Atienza-Moore, A. Chafin, and W. Vuono, all from NWC, for their contributions to this work. Their efforts, advice, and assistance are appreciated.

### References

1. Nielsen, A. T., R. L. Atkins, and W. P. Norris, "Oxidation of Poly(nitro)anilines to Poly(nitro)benzenes: Synthesis of Hexanitrobenzene and Pentanitrobenzene," *Journal of Organic Chemistry*, 44 (1979) pp. 1181-1182.
2. Nielsen, A. T., *et al.*, "Synthesis of Polynitro Compounds. Peroxydisulfuric Acid Oxidation of Polynitroarylamines to Polynitro Aromatics," *Journal of Organic Chemistry*, 45 (1980) pp. 2341-2347.
3. Nielsen, A. T., W. P. Norris, R. L. Atkins, and W. R. Vuono, "Nitrocarbons. 3. Synthesis of Decanitrobiphenyl," *Journal of Organic Chemistry*, 47 (1982) pp. 1056-1059.
4. Schischkoff, L., "Preliminary Notice on Quadruple Nitrated Types. Tetranitromethane," *Annalen*, 119 (1861) pp. 247-248.
5. Will, W., "Hexanitroethane," *Berichte*, 47 (1914) pp. 961-965.
6. Holden, J. R., D. A. Cichra, and C. Dickinson, "Estimation of 'Normal' Densities of Explosive Compounds from Empirical Atomic Volumes," Naval Surface Weapons Center, TR 79-273 (February 1980).
7. Rothstein, L. R. and R. Petersen, "Predicting High Explosive Detonation Velocities from Their Composition and Structure," *Propulsion and Explosion*, 4 (1979) pp. 56-60.
8. Nielsen, A. T., "Calculations of Densities of Fuels and Explosives from Molar Volume Increments," Naval Weapons Center, TP 5452 (February 1978).
9. Willer, R., "Synthesis and Characterization of 1,3,7,9-Tetranitro-1,3,7,9-Tetraazaspiro(4.5) Decane. TNSD," Naval Weapons Center, TP 4703 (March 1982).
10. Willer, R., "Synthesis of *Cis* and *Trans*-1,3,5,7-Tetranitro-1,3,5,7-Tetraazadecalin, Two New Energetic Materials," Naval Weapons Center, TP 6416 (January 1983).
11. Willer, R., "Synthesis of a New Explosive Compound, *Trans*-1,4,5,8-Tetranitro-1,4,5,8-Tetraazadecalin," Naval Weapons Center, TP 6303 (August 1982).
12. Coburn, M., "Picryl-substituted Heterocycles. II. Fuzans (1,2)," *Journal Heterocyclic Chemistry*, 5 (1968) pp. 83-87.
13. Komin, A. P., R. W. Street, and M. Carmack, "The Chemistry of 1,2,5-Thiadiazoles. III. (1,2,5)Thiadiazolo(3,4-)(1,2,5)Thiadiazole," *Journal of Organic Chemistry*, 40 (1975) pp. 2749-2751.
14. Visalok, I. V. and A. V. Ostrovskoya, "Preparation of Diaminofurazan," *Khimiya i Tekhnol Elementoorgan Soedin*, 78 (1978) pp. 48-49.
15. Willer, R., "Synthesis of a New Energetic Material, 1,4,5,8-Tetranitro-1,4,5,8-Tetraazadifurazano [3,4c]-[3,4-h]Decalin (CL-15)," Naval Weapons Center, TP 6397 (November 1982).
16. Kamlet, M. J. and S. J. Jacobs, "Chemistry of Detonations. I. A Simple Method of Calculating Detonation Properties of C-H-N-O Explosives," *Journal of Chemical Physics*, 48 (1968) pp. 23-25.

## Authors



Ronald Atkins is a supervisory research chemist. His research interests include the synthesis and characterization of new energetic materials for explosive, detonant, and propellant applications. He joined the staff of the NWC Research Department as a National Research Council Postdoctoral Research Associate in 1971 and is now the Head of the Energetic Materials Branch of the Chemistry Division. He received his Ph.D. from the University of New Hampshire, Durham.



Richard Hollins is a research chemist in the Energetic Materials Branch of the NWC Chemistry Division. His research specialties are organic synthesis, energetic materials synthesis, energy transfer, and laser dyes. His present research efforts include synthesis and characterization of polynitroaromatic explosives, new organic dye molecules for laser applications, and studies concerning the mechanism of phosphonate ester hydrolysis. He received his Ph.D. from the University of Oregon, Eugene.

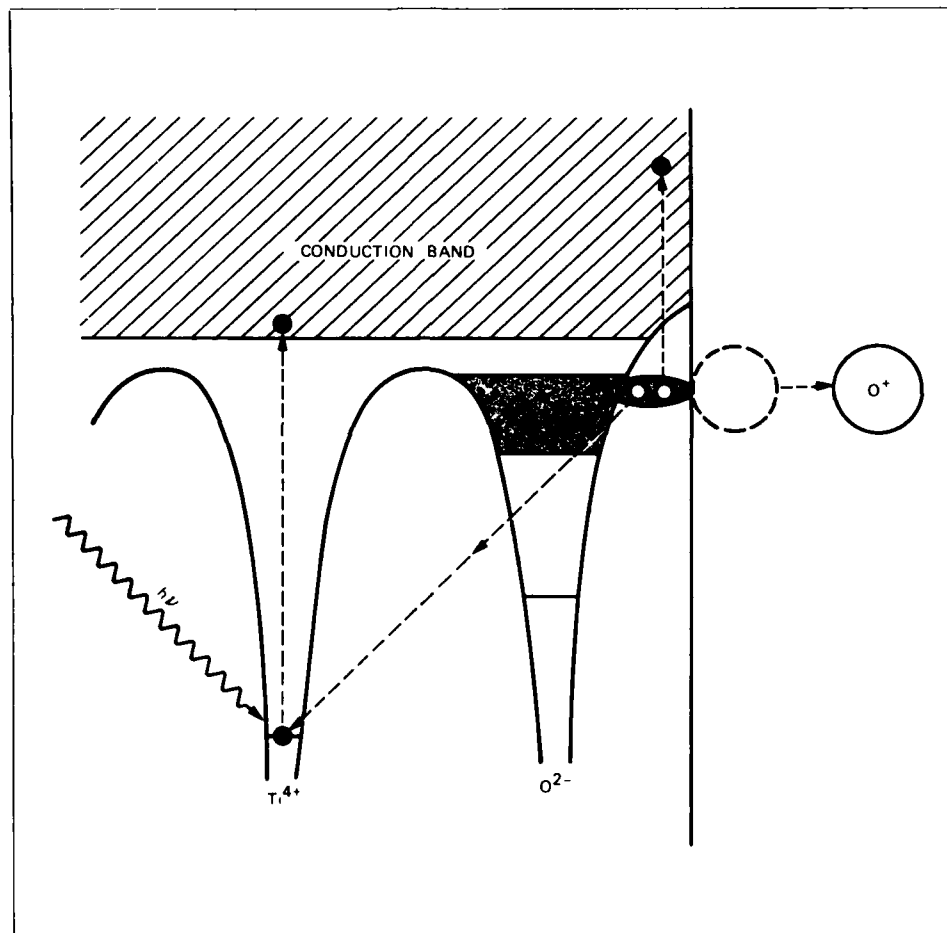
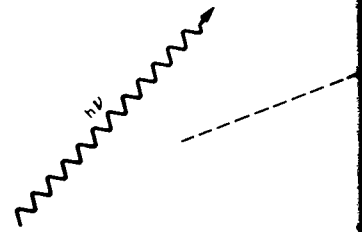


Arnold Nielsen is a senior research chemist on the staff of the NWC Chemistry Division. His current research interests include the synthesis and chemical behavior of energetic materials (explosives, propellant ingredients, and fuels) and the organic chemistry of polynitrogen compounds including stereochemistry and reaction mechanisms. His research is concerned with the synthesis of caged macrocyclic nitramine explosives and zero hydrogen explosives. He received his Ph.D. from the University of Washington, Seattle.

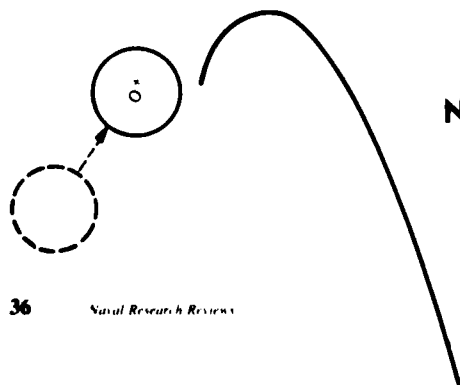


Rodney Willer is a research chemist in the Energetic Materials Branch of the NWC Chemistry Division. His research interests include synthesis of new energetic materials, structure elucidation and molecular dynamics by multinuclear-NMR spectroscopy, and conformational analysis of saturated heterocycles. His most recent research concerns the synthesis and characterization of macrocyclic and polycyclic nitramine explosives. He received his Ph.D. from the University of North Carolina, Chapel Hill.

# Surface Science with Photon-Stimulated Ion Desorption



by  
Victor Rehn  
Naval Weapons Center





## Introduction

Many physical processes within the outermost layers of atoms in solids differ from those deeper within the atoms' bulk material. Chemical, electronic, optical, mechanical, and other processes are changed in detail or effect by the asymmetrical surface environment of the atom or by interaction with the external ambient. For example, the (110) plane of a GaAs crystal contains Ga-As bonds lying within the plane when the plane is within the bulk. If the crystal is cleaved in vacuum along the (110) plane, the atoms rearrange themselves so that the Ga-As bond tilts out of the plane by about 28 degrees. Electronic changes occur along with this "reconstruction" of the (110) surface plane. The absence of neighboring atoms on the vacuum side frees bonding or valence orbitals on each atom so that the orbitals "dangle" in the vacuum. These surface dangling-bond states are eigenstates of the reconstructed two-dimensional surface lattice, but they are not eigenstates of the bulk crystal. Because they are not part of the bulk band structure, they may act to scatter or trap electrons from Bloch eigenstates of the three-dimensional crystal. Charges trapped in such surface or interface states are sources of electrostatic potential that affects the motion of charge carriers within hundreds of lattice spacings from the surface. In this way, the action of the outermost surface layer of an atom may influence charge transport or optical properties in a much larger region of the solid.

The study of the outermost layers of atoms is the domain of surface science. Many techniques are exploited in the study of surface or interface layers. Such layers may be reconstructed as a consequence not only of vacuum cleavage, but also of adsorption, oxidation, metal film deposition, heteroepitaxial growth, or other surface modifications. Most surface-science techniques involve stimulus-response measurements, using a probe beam to stimulate the surface layer. Usually, the surface response is observed by the emitted or scattered particles. Such experimental techniques may be categorized by the probe-beam particles and the detected particles, either of which may be ions (or atoms), electrons, or photons. Ideally, the probe beam should excite only one atomic layer with a single-quantum excitation, without causing significant damage or change in the surface. Ion probe beams penetrate least deeply into the solid, exciting the fewest layers but causing the greatest damage to the surface. Photon probe beams penetrate much more deeply, exciting many layers of atoms but stimulating mainly electronic, single-quantum excitations and causing little or no atomic disorder in the surface. Electron probe beams penetrate quite deeply, causing some atomic disorder while inducing a variety of electronic excitations by inelastic scattering. No probe beam approaches the ideal of single-layer, single-quantum excitation without irreversible disturbance to the surface.

Ideally, detected particles should carry information about an undisturbed single layer of surface atoms or, even more specifically, about a particular atomic site in the surface layer. Generally, the emitted low-energy ions represent the outermost surface layer, while the electrons or photons emitted

represent electronic excitations. Again, none of the detected particles ideally represents specific excitations of the surface atomic layer alone, but combinations of the probe-beam particles and the detected particles provide valuable information about the surface layer of atoms.

Just as point defects in the bulk crystal may control or dominate the electrical or optical properties of crystals, point defects on the crystal's surface may strongly influence the electrical and optical properties of the surface. For example, plots of optical absorption versus thickness usually show a nonzero intercept, representing an absorption associated with the surfaces. Usually this absorption is ascribed to imperfections, including chemical impurities, in the surface layers that are not distributed throughout the bulk. Electronic or vibrational excitations of surface imperfections are observed in surface optical absorption measurements. However, detailed theory of surface optical absorption is in a primitive state because of the difficulty of measuring and calculating the electronic states associated with surface point defects. Only recently, surface-science measurement techniques that are sensitive to such localized states in surface layers have become available. Two of these techniques are surface-extended, x-ray-absorption fine structure (SEXAFS) and photon-stimulated ion desorption (PSID<sup>\*</sup>). Both of these techniques provide sensitivity to the outermost surface layer, and PSID also provides sensitivity to isolated point defects.

## SEXAFS Techniques

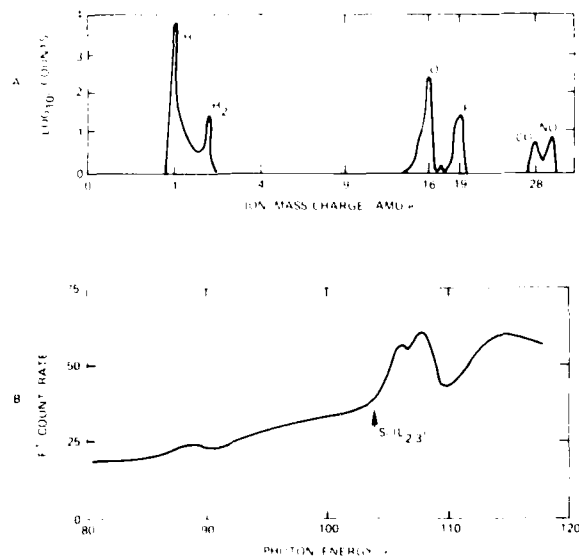
The use of ordinary extended x-ray absorption fine structure (EXAFS) techniques does not provide surface sensitivity because of the deep penetration of x-rays into the crystal. However, in SEXAFS techniques surface sensitivity is provided by detecting the photoelectron yield (PEY), instead of the transmitted x-rays resulting from soft x-ray excitation. By detection of PEY, the x-ray absorption within the photoelectron escape depth (4-10 Å) is monitored as a function of photon energy. Careful analysis of SEXAFS data provides near-neighbor interatomic distances around the surface-excitation site. For example, if the spectral region above the As ( $M_{2,3}$ ), or 3s, absorption edge is studied on a GaAs (110) surface, the Ga-As bond length and possibly the As-As separation may be obtained on the reconstructed surface. Such a study may be made as the surface is exposed to oxygen, sub-monolayer metal coverage, elevated temperature, ionizing radiation, or other stimuli that may influence the interatomic distances in the surface region.

In principle, SEXAFS measurements could be used to probe the environments of isolated atoms on surfaces (such as Au atoms on GaAs), or specific groups of photoelectrons (such as angle- or energy-resolved photoelectrons) could be detected in place of the total PEY. In practice, the SEXAFS signal is too weak to permit observation with the reduced signal strength

\*PSID is sometimes referred to as "PSD" in analogy with electron-stimulated desorption (ESD)

**Figure 1**

PSID results on a co-evaporated Nb<sub>3</sub>Sn thin film after a 500°C bake in vacuum. Part A shows the time-of-flight mass spectrum of photoemitted positive ions. Both molecular and atomic surface impurities may be observed. Part B shows a representative excitation spectrum. By observing that F\* emission shows a strong threshold at the Si(L<sub>2,3</sub>) excitation energy, three levels of knowledge result. (1) analysis: Si and F are present on the Nb<sub>3</sub>Sn surface. (2) chemistry: F bonds to Si impurity atoms on the Nb<sub>3</sub>Sn surface. (3) physics: the spectral shape of the near-edge structure may be analyzed to study the electronic structure at the Si-F surface-impurity site on Nb<sub>3</sub>Sn (see reference 4).



these measurements would require. SEXAFS is used in the study of sites of majority species on the surface, but not to study the sites of minority species. To study the structure and electronic states at sites of minority species on the surfaces, PSID may be used. The remainder of this paper will deal with PSID and its applications.

## PSID Techniques

Exploiting the single-quantum excitation characteristic of the photon-probe beam and the single-layer sensitivity of emitted low-energy ions, PSID techniques facilitate the study of a variety of structural and electronic features of isolated surface sites. In PSID measurements, low-energy ions that are emitted or "desorbed" from the surface are identified by charge-to-mass ratio using a time-of-flight or other mass analyzer.<sup>1</sup> The excitation-energy spectrum for each ionic species emitted is obtained by using a scanning monochromator in the photon-probe beam. Empirically, it has been found that the probability of PSID is very low, below 10-15 eV, and that photon-excitation thresholds for ion emission coincide with the *core-excitation* energies of surface-site atoms.<sup>2</sup> Thus, PSID has been shown to result from a single-quantum excitation of an atomic-core electron.

Because the kinetic energy of the emitted ion is so low ( $Z < 10$  eV), it is concluded that the ions issue from the outermost surface layer. The emission of higher-energy ions after energy loss by collisions is ruled out by time-resolved results and by the emitted-ion kinetic-energy spectrum. Time-resolved results show that any delay time for an energy-loss process must be less than  $10^{-12}$  sec and must be independent of excitation energy above the threshold energy. Emitted-ion kinetic-energy spectra are generally peaked and do not show the marks of a collisional energy-loss process. Thus PSID measurements detect ions from the outermost layer of surface atoms as stimulated by a single-quantum atomic-core excitation.

Isolated sites in the surface layer may be studied by PSID in two ways. Isolated-surface impurity atoms may be identified directly among desorbing species, or indirectly as surface sites for other desorbing species. Both methods of identification are needed for a complete study of all the chemical impurities on surfaces because of the wide variation in the desorption probability for various atoms. Singly bonded atoms, such as Group I or Group VII atoms, are readily desorbed while multiply-bonded atoms are seldom desorbed. Multiply-bonded atoms are studied as PSID sites. With two complementary methods, many surface impurities can be studied using PSID techniques.<sup>3</sup>

## Surface Chemical Analysis of Superconducting Thin Films

Electronic devices using superconductors have demonstrated extremely fast switching times ( $< 10^{-11}$  s). Superconducting microwave cavities have extremely low loss (1/Q

$< 10^{-9}$ ). Superconducting magnetometers are capable of detecting magnetic-field changes  $< 10^{-12}$  T. With such capabilities, it seems remarkable that superconducting devices are not more widely used in both commercial and military applications. Problems impeding the broader application of superconducting devices involve both the difficult materials technology and the costly cryogenic technology. If reliable superconducting devices can be fabricated from high-T<sub>c</sub> superconductors such as Nb<sub>3</sub>Ge or Nb<sub>3</sub>Sn, both cost and performance factors will improve; materials-technology development is the keystone.

Traditionally, superconducting materials have been considered sensitive to metallurgical treatment, which affects crystal structure, but insensitive to the trace chemical impurities that dominate semiconductor properties. On the other hand, the Josephson-junction device derives its dramatic performance from the interaction of superconducting charge carriers (Cooper pairs) with a thin insulating barrier. Tunnel currents through the barrier depend on barrier parameters, mainly thickness and height. The barrier height, in turn, depends on the chemical composition and purity of the extremely thin tunnel barrier, which is usually  $< 50$  Å thick. Thus, in Josephson-junction or similar devices, minor impurities on superconductor surfaces may play an important role in the performance of the device.

The first PSID study of chemical impurities on Nb and Nb<sub>3</sub>Sn surfaces clearly illustrated the complex surface chemistry involved.<sup>4</sup> In all, 23 impurities were identified by PSID, while only carbon and oxygen were identifiable by Auger electron spectroscopy. Hydrogen and oxygen are expected to be of greater significance in tunnel-junction performance, especially if the oxidized amorphous-silicon (a-Si) barrier is used. Further studies are being carried out on the roles of these impurities, both in the growth of high-quality Nb<sub>3</sub>Ge films and in the formation of tunneling barriers of oxidized a-Si on high-T<sub>c</sub> superconducting films (Figure 1).

### Hydrogen Interaction With (110) Surfaces of Group III-V Compound Semiconductors

As mentioned in the introduction, electronic surface states on semiconductors may trap or scatter charge carriers even though the charge carriers are in Bloch eigenstates of the three-dimensional crystal. For this reason, the control of surface electronic states is important in electronic devices, and increasingly important as the device speed is increased or the device size is reduced. One of the simplest chemical agents for surface-state control is hydrogen, which forms a single, simple covalent bond with many atomic species. Although the room-temperature reactivity of hydrogen with Group III-V semiconductor surfaces is low, the high sensitivity of PSID to hydrogen facilitates the study of very small amounts of surface hydrogen (Figure 2).

**Figure 2**

Atomic Sites on the (110) surface of Group III-V compound semiconductors. The surface lattice shown (bold lines) is the (110) plane of the truncated crystal (of zinc-blende structure). Group III atom sites are represented by solid circles and Group V atom sites on the surface are represented by open circles. In the "reconstruction" of the clean surface, all Group III surface atoms sink slightly into the crystal, and all Group V surface atoms rise slightly out of the crystal. This reconstruction results in the tilting of the Group III-V surface bond out of the surface plane by about 28 degrees. Each surface atom has one free bond "dangling" out of the crystal because of the absence of the next atomic layer. Electronic shifts cause the dangling bond of the Group III atom to be unoccupied (above the Fermi energy), its electron shifting to fill the dangling bond of the Group V atom, which lies energetically deep in the valence band.

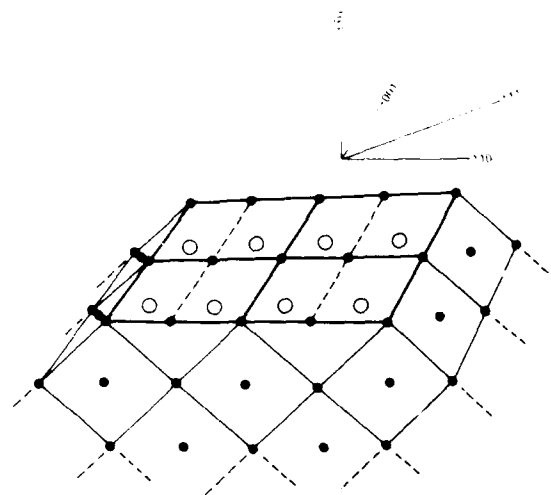
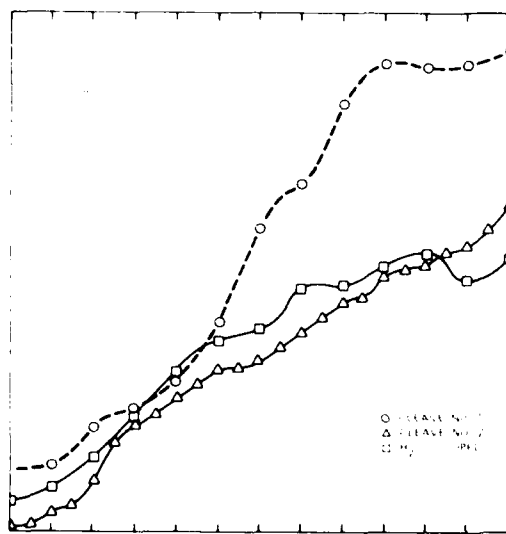


**Figure 3**

$H^+$  PSID excitation spectra of cleaved (110) GaAs. Hydrogen dissolved in GaAs during crystal growth is bonded to Ga surface atoms on freshly cleaved surfaces. The excitation thresholds shown near 20 eV correspond to Ga ( $M_{2,3}$ ) or 3d excitation at the surface Ga-H site. Exposing the surface to  $H_2 O$  vapor produces an additional  $H^+$  desorption threshold at 23 eV, corresponding to O(1s) or 2s excitation of the surface OH adsorbate (see reference 5).



The study of the hydrogen interaction with surface dangling bonds begins with the study of freshly cleaved, clean semiconductor surfaces. Group III-V semiconductors cleave along (110) crystal planes. Such clean surfaces are prepared *in situ* in ultrahigh vacuum, where surfaces contaminate slowly over a period of hours by interaction with ambient gas molecules. PSID on such freshly-cleaved, clean surfaces shows little or no ion yield because the multiply-bonded Group III-V elements are seldom desorbed. An exception was found for GaAs crystals grown in a hydrogen environment. The freshly cleaved surfaces of these crystals showed considerable  $H^+$  desorption when the Ga( $M_{2,3}$ ) or 3d, core states were excited<sup>5</sup> (Figure 3).

The interaction of hydrogen with InP (110) surfaces was studied using PSID and total PEY. A low pressure stream of excited, molecular hydrogen ( $H_2^*$ ) was flushed across the freshly cleaved surface to an exposure level of  $10^4 L$ .<sup>†</sup> PSID and total PEY excitation spectra were then studied above the P(K) and In(L) excitation thresholds.<sup>6</sup> The total PEY spectrum was nearly unchanged by the  $H_2^*$  exposure, while the PSID results showed  $H^+$  desorption spectra with thresholds at P(K) and at the three In(L) edges. Using the total PEY spectra near these edges as a measure of the photoabsorption in the surface region, it was deduced that the population of In-H surface bonds and P-H surface bonds is in the same order of magnitude. Previous studies of the GaAs (110) surface indicated a similar result. Thus, the reactivity of  $H_2^*$  with Group III and Group V elements on (110) surfaces appears to be approximately equal (Figure 4).

This result suggests a model for hydrogen-surface interaction involving the dangling-bond states. The  $H_2$  molecule has two electrons, and two more electrons are found in the P dangling bond, facilitating the formation of adjacent In-H and P-H bonds. At the same time, the establishment of similar electron densities around the In and P surface atoms by the adsorption of hydrogen removes the cause of the bond tilt, and the In-P bond is expected to return to the (110) plane as in the bulk crystal (Figure 5).

The hydrogen dosage used in these experiments ( $10^4 L$ ) was far less than needed to completely cover the surface with hydrogen. Although the hydrogen coverage is unknown, it is expected to be less than 0.01 monolayer, possibly much less. Published research on the interaction of oxygen with GaAs under similar circumstances led to conclusion that a dose of more than  $10^{10} L$  of  $O_2^*$  would be necessary to completely cover the surface. Our results on hydrogen chemisorbed on InP, GaP, and GaAs surfaces probably represent isolated hydrogen surface sites or small covered areas. To test the hydrided surface for transport properties, we must learn to produce stable, complete coverage of the surface. If such coverage of the surface can be done, surface trapping and scattering of charge carriers at hydrided Group III-V semiconductor surfaces may be expected to be reduced because the surface dangling bonds are used in covalent bonds similar to the bulk bonds.

<sup>†</sup> L. = Langmuir, a unit of exposure equivalent to  $10^{-6}$  torr seconds.

**Figure 4**

Total PEY and PSID excitation spectra compared at the P(K) and In(L) edges on hydrogen-dosed InP (110) (see reference 6)

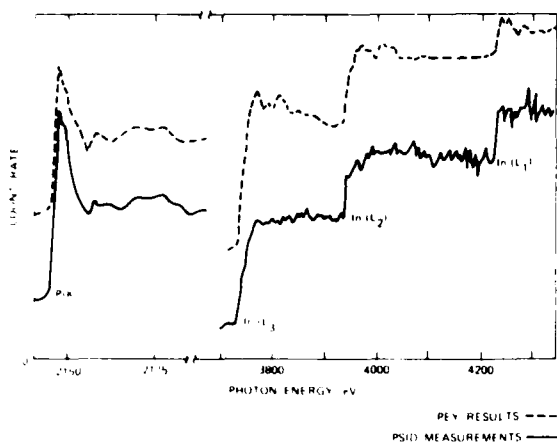
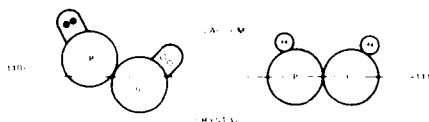


**Figure 5**

Model for hydrogen surface sites on InP. The left-hand In-P bond is shown tilted as appropriate to a clean InP (110) surface with surface dangling bonds. On the right, hydrogen is shown bonded to adjacent In and P surface atoms. Both dangling bonds are now occupied and the electronic symmetry restores the bulk-crystal positions of the atoms (see reference 6)



## References

1. Knotek, M. L., V. O. Jones, and Victor Rehn, "Photon-Stimulated Ion Desorption by Excitation of Deeper-Lying Core Levels: Density of States and Extended Fine Structure," *Surface Science*, 102 (1981) p. 566.
2. Rosenberg, R. A., Victor Rehn, A. K. Green, P. R. LaRoe, and C. C. Parks, "Photon-Stimulated Ion Desorption from Condensed Molecules: N<sub>2</sub>, CO, C<sub>2</sub>H<sub>2</sub>, CH<sub>3</sub>OH, N<sub>2</sub>O, D<sub>2</sub>O, and NH<sub>3</sub>," *Proceedings First International Workshop on Desorption Induced by Electronic Transitions — DIET-1*, Editors, N. Talk, M. Traum, T.E. Madey and J.C. Tully. (Springer-Verlag, 1982) p. 197.
3. See, for example, *Proceedings First International Workshop on Desorption Induced by Electronic Transitions — DIET-1*, Editors, N. Talk, M. Traum, T.E. Madey and J.C. Tully. (Springer-Verlag, 1982) p. 197.
4. Rehn, Victor, A. K. Green, R. A. Rosenberg, G. M. Loubriel, and C. C. Parks, "The Chemical Makeup of Nb and Nb<sub>3</sub>Sn Films," *Physica* 107B (1981) p. 533.
5. Thornton, G., R. A. Rosenberg, Victor Rehn, A. K. Green and C. C. Parks, "Photon-Stimulated Ion Desorption of H<sup>+</sup> Ions from GaAs(110)/H<sub>2</sub>O," *Solid State Communications* 40 (1981) p. 131.
6. Rehn, Victor, R. A. Rosenberg, P. J. Love, P. R. LaRoe, A. K. Green, and C. C. Parks, "Photon-Stimulated Ion Desorption and Photoemission Yield Studies of Clean and Hydrided (110) Surfaces of GaP and InP," presented at the Japan-USA Seminar on Recombination-Induced Defect Formation, University of Illinois at Urbana, (2-5 June 1982) to be published.

## Author



Victor Rehn obtained his Ph.D. (Physics) from the University of Pittsburgh in 1962, specializing in solid state physics. He has been employed as a research physicist at the Naval Weapons Center since 1965, and now serves as head of NWC's Semiconductor and Surface Science Branch. In 1981, Dr. Rehn received the L.T.E. Thompson Award for the discovery of photon-stimulated ion desorption and leadership in the Michelson Laboratory Synchrotron Radiation Project (MLSRP). His current research interests include the optical properties of materials and the surfaces and interfaces of semiconductor materials and their interaction with adsorbates.

## Profiles in Science



**JOHN PEARSON** has received national and international recognition for his work in the interaction of explosives and metals for both industrial and military applications. His pioneering work in explosive forming and explosive welding has contributed greatly to explosives and materials research and has earned him a reputation as the "father of explosive forming and welding." His research has also included the extension of shaped-charge theory to new ordnance applications and the development and application to warheads of new fragmentation-control theories. Mr. Pearson completed his B.S. degree in Mechanical Engineering and M.S. degree in Applied Mechanics at Northwestern University following military service during World War II.

Mr. Pearson came to the Naval Weapons Center (then the Naval Ordnance Test Station) in 1951. He started his career at China Lake as a research engineer in the Physics Division of the Research Department, where he began a long and productive relationship with Dr. John Rinehart, another pioneer in explosives research. Soon Mr. Pearson was selected to head the Warhead Research Branch of the Propellants and Explosives Department. Even at NOTS the branch was a unique organization, as it included both civilian and military personnel and contained its own laboratories, shops, and test facilities. It was also known for quick-response capabilities

and significant contributions to the field of explosive ordnance.

In 1959 Mr. Pearson returned to the Research Department as head of the Detonation Physics Group and later moved to the Detonation Physics Division, which he continues to head as a career rehired annuitant since his 1980 retirement. His continued growth and his remarkable ability to combine research with engineering discipline and perspective make John Pearson vital to the Navy today as well as its future missions.

Mr. Pearson has authored or coauthored over 100 technical publications and three books. Two of the books, which he coauthored with Dr. Rinehart, have become classics in their field: *The Behavior of Metals Under Impulsive Loads*, and *Explosive Working of Metals*. Mr. Pearson is a charter member of the Senior Executive Service of the United States; a national lecturer for the American Society for Metals, the American Society of Mechanical Engineers, and the American Society of Tool and Manufacturing Engineers; and a Fellow of the American Society of Mechanical Engineers. He has received both the L.T.E. Thompson Award, in recognition of outstanding contributions to the advancement of ordnance, and the William B. McLean Award, in recognition of outstanding creativity as evidenced by significant inventions.

# The Michelson Laboratory Synchrotron Radiation Project

by

Victor Rehn  
Naval Weapons Center

The Michelson Laboratory Synchrotron Radiation Project (MLSRP) originated at the Naval Weapons Center (NWC) in 1972 to exploit synchrotron radiation (SR) in the study of electronic materials that have potential for Navy application. In the decade since 1972, many types of SR experiments have been conducted involving nearly two dozen NWC scientists. Each of the remarkable properties of SR has been exploited: the high-intensity, highly polarized, low-noise continuum spectrum (visible to x-ray), the ultraclean, ultrahigh vacuum environment, the subnanosecond radiation pulses with a 1.28-MHz repetition rate, and the highly collimated small beam. MLSRP continues under NWC and Office of Naval Research (ONR) funding, with current emphasis on surface studies using photon-stimulated ion desorption described in another article, "Surface Science With Photon-Stimulated Ion Desorption," in this issue.

The project had its origin in August 1972 at a Gordon Conference on high-energy spectroscopy, where interest was in band-structure analysis for wide-gap semiconductors and insulators. Professor F. C. Brown of the University of Illinois mentioned SPEAR, the newly built Stanford positron-electron acceleration ring, as a potentially wonderful source of SR for vacuum-ultraviolet (VUV) spectroscopy. Later Professor W. E. Spicer of Stanford University agreed that a collaboration in the construction of experimental facilities and subsequent experiments on VUV reflectance and modulation spectroscopies would be welcomed. In subsequent meetings with management personnel at NWC and Stanford, the basis for collaboration and funding proposals was formulated. In November 1972, a proposal was submitted by NWC requesting funding for a joint NWC-ONR project in VUV SR research in electronic materials.

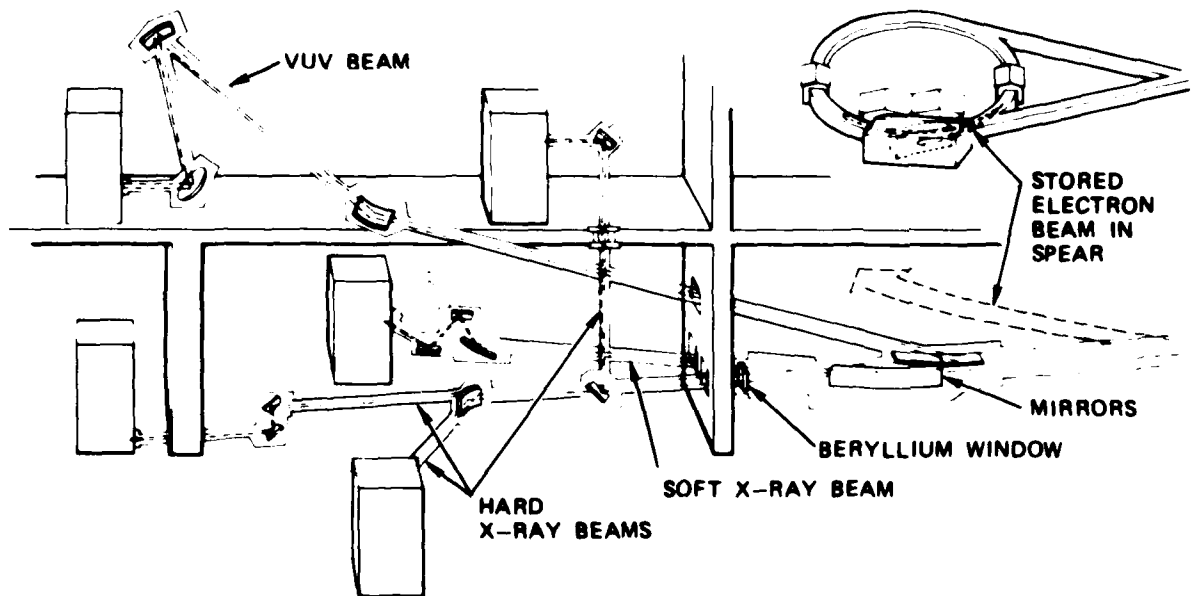
In early February 1973, ONR funding was received. The project began in earnest. Professor S. Doniach of Stanford and Dr. Spicer formed similar collaborations with Dr. Brown, then at the Xerox Palo Alto Research Center, and with Professor J. Baldeschwieler of the California Institute of Technology. In June 1973, the Stanford SR project (SSRP), was funded by the National Science Foundation (NSF) on the basis that NSF would fund the building construction, the control and safety systems, and the modifications necessary in the SPEAR ring. Each of the collaborating groups was responsible for one beam line and was to be granted priority for initial use of that beam line after official opening of the experimental program. NWC was responsible for the VUV beam line (now called the 8-degree branch line or beam line 1-2) and mirror design and procurement for the soft x-ray beam line built by the Xerox group (Figure 1). In November 1973, P. Eisenberger of Bell Laboratories joined the collaboration to build an extended x-ray absorption fine structure (EXAFS) station. By November 1974, all five experiment stations were functioning, and an exciting variety of SR experiments at SSRP\* was beginning.

Among the MLSRP accomplishments of the past eight years was the measurement of the VUV transmission and reflection spectra of lithium yttrium fluoride,<sup>1</sup> LiYF<sub>4</sub>, and the

\*SSRP is now called "Stanford Synchrotron-Radiation Laboratory (SSRL)," and is a national facility for research using synchrotron radiation. Funded by Department of Energy, SSRL is available to all qualified users, and has been used by more than 700 scientists.

**Figure 1.**

Beam lines of the original SSRP. This complex of five branching beam lines is now referred to as beam line 1. Although MLSRP constructed only the VUV beam line, currently MLSRP is a "user" of all SSRL beam lines appropriate to the experimental requirements.



VUV reflectance and scattering spectra of various SiC materials.<sup>2</sup> The former experiment showed LiYF<sub>4</sub> to have a fundamental absorption edge at 10.5 eV (1185 Å), making it competitive with LiF and MgF<sub>2</sub> among UV transmitting materials. The SiC results helped to establish its remarkable optical properties and led to its growing use for mirrors or mirror substrates. Other achievements were the study of fluorescence excitation and emission spectra of matrix-isolated small molecules by time-resolved spectroscopies,<sup>3</sup> and the study of VUV and soft x-ray scattering of real mirror surfaces.<sup>4</sup>

The highlight was the discovery of photon-stimulated ion desorption (PSID) in December 1978.<sup>5</sup> M. L. Knotek of Sandia Laboratories had presented the Knotek-Feibelman model for electron-stimulated ion desorption from fully valent ionic solids. In this model, the first step is creation of a core hole in a surface atom by inelastic electron scattering. Knotek and I were convinced that the subsequent events leading to ion desorption were independent of the mechanism of creation of the core hole. I suggested that this idea could be tested using SR, and that the NWC apparatus for angle-resolved scattering together with the time-resolved spectroscopy electronic system could be adapted for the test. I pointed out the advantages of time-of-flight mass spectroscopy for noise reduction and for identification of emerging ionic species. Seventy-two hours of beam time in December 1978 were "bootlegged" for the test. The predictions were confirmed. H<sup>+</sup>, OH<sup>+</sup>, and O<sup>+</sup> ions were observed to desorb from a TiO<sub>2</sub> crystal surface, after reducing, ion etching, and exposing the surface of H<sub>2</sub>O vapor.<sup>5</sup> Since that time PSID has been applied to the study of semiconductors, insulators, metals, superconductors, molecular solids, and adsorbed layers. A wide variety of scientific phenomena has been investigated, including surface chemical analysis, surface bonding, photoionization processes, adsorbate-surface chemical reactions, surface dangling-bond charging, and photolysis.

MLSRP has also produced important results of a less tangible nature. For example, attention was drawn to the potentialities and technical problems of free-electron lasers for military applications and to certain special materials, such as SiC for optical components for high-energy lasers. Closer interactions were fostered between NWC and university or industrial laboratories, both here and abroad. These interactions include interdisciplinary ones that grew from the heterogeneous mix of specialists who use SR in their research. This symbiotic laboratory environment may turn out to have as great a benefit to the U.S. technological community as will the scientific discoveries made in the SR laboratory.

## Acknowledgements

The author wishes to acknowledge the major contributions to the MLSRP that were made by the other members of the original MLSRP group: V. O. Jones, D. S. Kyser, J. L. Stanford. Other NWC scientists who made significant contributions to the project are as follows: T. E. Anderson, A. D. Baer, J. M. Bennett, D. L. Burdick, D. K. Burge, R. L. Chapman, L. F. DeSandre, J. M. Elson, A. K. Green, J. L. Jernigan, P. J. Love, K. M. Monahan, A. J. Nelson, J. P. Rahn, R. A. Rosenberg, R. W. Schwartz, and D. J. White.

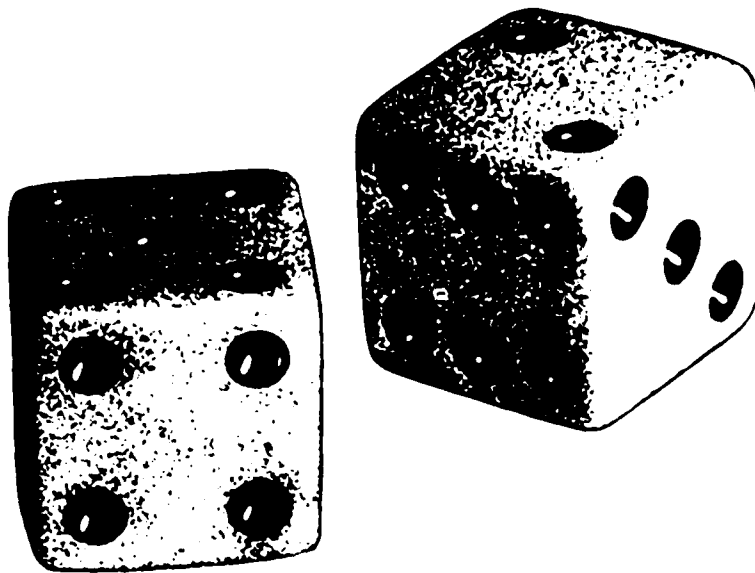
## References

1. Rehn, Victor, D. L. Burdick, and V. O. Jones, "UV Reflectance, Transmission and Photoluminescence of LiYF<sub>4</sub> and the Bulk Loss Coefficient in CaF<sub>2</sub>," *Laser Induced Damage in Optical Materials*, Editors, A. J. Glass and A. H. Guenther, Washington, D.C., National Bureau of Standards, NBS Special Publications 509 (1977) p. 132.
2. Rehn, Victor, and W. J. Choyke, "SiC Mirrors for Synchrotron Radiation," *Nuclear Instrumentation Methods*, 177 (1980) p. 173.
3. Monahan, K. M., V. O. Jones, and Victor Rehn, "Photodissociation of XeF<sub>2</sub> in Solid Xe and Kr," *Journal of Chemical Physics*, 71 (1979) p. 2360.
4. Elson, J. M., Victor Rehn, J. M. Bennett, and V. O. Jones, "Measurement of Angle-Resolved Light Scattering From Optical Surfaces in the 75-750 eV Range," *Proceedings SPIE*, 315 (1982) p. 193.
5. Knotek, M. L., V. O. Jones, and Victor Rehn, "Photon-Stimulated Desorption of Ions," *Physical Review Letters*, 43 (1979) p. 300.

# The Mathematics of Simple Random Walks

by

Daniel T. Gillespie  
Naval Weapons Center



## Introduction

Many real-world processes contain some element of randomness. When this random element is so strong that the course of the process is not uniquely determined by knowable parameters, the process is said to be *nondeterministic*. The best known examples of a nondeterministic process are games of chance, such as craps or roulette. Some examples of a more pressing concern to the Navy are the depletion of weapons stores on a combat ship and the evolution of a complex war game. Nondeterministic processes also abound in the physical sciences. For example, since we cannot track all molecular positions and velocities in a gas of many thermally colliding molecules, it follows that the evolution of a gas-phase chemical reaction is basically a nondeterministic process.

In a *deterministic* process, the state  $S(t)$  of the system at any time  $t$  suffices to uniquely determine the state  $S(t + dt)$  at

an infinitesimally later time  $t + dt$ . This fact allows construction of a differential equation for the state function  $S$ , and if the state of the system at some initial time is specified, the corresponding solution of that differential equation unambiguously gives the state at any later time. But if the process is *nondeterministic* — e.g., if a knowledge of  $S(t)$  permits only a *probabilistic* prediction to be made of  $S(t + dt)$  — this traditional analytical approach clearly does not work.

The analysis of nondeterministic processes has been the focus of a small but persistent investigative effort in the independent research program at the Naval Weapons Center. One of the main goals has been simply to learn and develop basic mathematical approaches and techniques. In that somewhat tutorial spirit, we shall review here some of the mathematical ways of analyzing one simple kind of nondeterministic process. Although our presentation contains much that is well known, it also incorporates many clarifications and new results developed in our research program.

## A Simple Random Walk Model

We consider a system whose possible states can be put into a one-to-one correspondence with the non-negative integers  $x$ . Furthermore, we suppose that the time evolution of the system is governed by two given functions,  $a_+(x)$  and  $a_-(x)$ , according to the following scheme:

$$a_+(x) dt \equiv \text{the probability that the system, if in state } x \text{ at time } t, \text{ will jump to state } x \pm 1 \text{ in the next infinitesimal time interval } (t, t+dt). \quad (1)$$

$(x=0, 1, 2, \dots)$

We shall assume that  $a_-(0)=0$ , so that the system stays off the negative  $x$ -axis.

One example of such a system is a mixture of chemically reacting molecules in which the populations of all but one reactant are held constant; in that case,  $x$  gives the current number of molecules of the unconstrained species, and  $a_+(x)$  and  $a_-(x)$  are the probabilities per unit time of chemical reactions which, respectively, create and destroy one of those molecules. Another example is a bound cluster of  $x$  molecules floating in a vapor of single molecules; in that case,  $a_+(x)$  and  $a_-(x)$  are the probabilities per unit time for the cluster to condense and evaporate a molecule.

Mathematically, our model is an example of a "continuous-time, discrete-state Markovian process." The term "Markovian" conveys the fact that the random behavior of the system is independent of its past; this is true because the probabilities in equation (1) depend at most on the current state  $x$  and not on how the system got to that state. Equation (1) implies that the state of the system moves about on the  $x$ -axis in sudden, irregular jumps from one integer to another. It is customary to refer to such behavior as a "random walk," and to the system itself as the "walker." Our particular random walk is further constrained to be a "single-variable, single-step" random walk, since the state of the walker is specified by a single variable that can change by only one unit at a time.

## The Master Equation

One way to mathematically describe our random walk model is to focus on the function

$$P(x,t) \equiv \text{the probability that the system will be in the state } x \text{ at time } t. \quad (2)$$

We can obtain a time-evolution equation for  $P$  by first expressing  $P(x,t+dt)$  as the sum of the probabilities of the three possible routes to being in state  $x$  at time  $t+dt$ :

$$P(x,t+dt) = P(x-1,t) \cdot a_+(x-1) dt + P(x+1,t) \cdot a_-(x+1) dt + P(x,t) \cdot [1 - a_+(x)dt - a_-(x)dt].$$

Here, the first term on the right is the probability that the system is in state  $x-1$  at time  $t$  and then jumps up one state in the next  $dt$ ; the second term is the probability that the system is in state  $x+1$  at time  $t$  and then jumps down one state in the next  $dt$ ; the third term is the probability that the system is already in

state  $x$  at time  $t$  and then does not jump at all in the next  $dt$ . A simple algebraic rearrangement leads to the following time-evolution equation for the function  $P$ :

$$\partial P(x,t)/\partial t = P(x-1,t)a_+(x-1) + P(x+1,t)a_-(x+1) - P(x,t)[a_+(x) + a_-(x)]. \quad (3)$$

This differential-difference equation is called the *master equation*. Although it is easy to derive, it is usually extremely difficult to solve.

If  $f$  is any function of the state  $x$ , then the average or expected value of  $f$  at time  $t$  is

$$\langle f(x) \rangle_t \equiv \sum_x f(x)P(x,t).$$

The  $n^{\text{th}}$  moment of  $P$  is defined to be  $\langle x^n \rangle_t$ . Of particular interest are  $\langle x \rangle_t$ , the average of  $x$  at time  $t$ , and  $[\langle x^2 \rangle_t - \langle x \rangle_t^2]^{1/2}$ , the standard deviation of  $x$  at time  $t$ ; the latter is a measure of the expected difference between an observed value of  $x$  at time  $t$  and the average  $\langle x \rangle_t$ . Multiplying equation (3) by  $x^n$  and then summing over  $x$ , we obtain the following time-evolution equation for the moments of  $P$ :

$$d\langle x^n \rangle_t/dt = \langle a_+(x) [(x+1)^n - x^n] \rangle_t - \langle a_-(x) [x^n - (x-1)^n] \rangle_t. \quad (4)$$

For  $n=0$  this equation shows that the time evolution specified by equation (3) is consistent with the normalization requirement,  $\sum_x P(x,t) = 1$ . For  $n=1$  equation (4) gives

$$d\langle x \rangle_t/dt = \langle a_+(x) - a_-(x) \rangle_t. \quad (5)$$

For  $n \geq 1$  we have a problem with equation (4) if either  $a_+(x)$  or  $a_-(x)$  is nonlinear in  $x$ . In that case the right side will contain  $\langle x^m \rangle_t$  for some  $m > n$ , thereby rendering the set of equations infinitely open-ended. Unfortunately, no known general procedure exists for solving such a set of equations.

If the functions  $a_+(x)$  and  $a_-(x)$  are everywhere positive [except that  $a_-(0)=0$ ] and satisfy  $a_+(x)/a_-(x) \rightarrow 0$  as  $x \rightarrow \infty$ , then it can be shown that  $P(x,t) \rightarrow P_\infty(x)$  as  $t \rightarrow \infty$ , where the function  $P_\infty$  is independent of both  $t$  and the initial state of the walker. (This of course does *not* imply that the walker eventually stops walking.) Equation (3) evidently requires that  $P_\infty$  satisfy

$$0 = P_\infty(x-1)a_+(x-1) + P_\infty(x+1)a_-(x+1) - P_\infty(x)[a_+(x) + a_-(x)].$$

A simple transposition of terms reveals that the quantity  $P_\infty(x)a_-(x) - P_\infty(x-1)a_+(x-1)$  must be a constant for all  $x$ , and taking  $x=0$  shows that this constant must be zero. Thus,

$$P_\infty(x) = [a_+(x-1)/a_-(x)]P_\infty(x-1), \quad (x=1, 2, \dots) \quad (6)$$

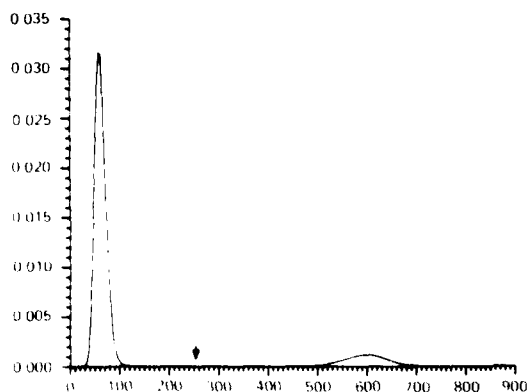
This is a simple recursion relation for  $P_\infty$ , iteration of which gives

$$P_\infty(x) = P_\infty(0) \prod_{n=1}^x [a_+(n-1)/a_-(n)], \quad (x=1, 2, \dots) \quad (7)$$

The quantity  $P_\infty(0)$  may be obtained from equation (7) and the normalization condition,  $\sum_x P_\infty(x) = 1$ .

**Figure 1**

The function  $P_x(x)$  for a bistable system.<sup>26</sup>



The extrema of the function  $P_x$  may be found (to within one unit of  $x$ ) by setting its "derivative"  $[P_x(x) - P_x(x-1)]/1$  equal to zero and then solving for  $x$ . Using equation (6), we can easily show that the extrema of  $P_x$  are those points  $x$  for which

$$a_-(x-1) - a_+(x) = 0. \quad (8)$$

Since the walker spends more time near states where  $P_x$  is large, the *local maximums* of  $P_x$  are of special importance; they are called the *stable states* of the system.

For explicit functions  $a_+$  and  $a_-$ , we can easily calculate the function  $P_x$  on a digital computer directly from the recursion relation equation (6). Figure 1 shows a computer-generated plot of  $P_x$  for a particular model in which equation (8) is a cubic with three distinct roots. This system evidently has two stable states, one at  $x_1 \approx 60$  and the other at  $x_2 \approx 600$ . Although it is not evident on this plot,  $P_x(x)$  is strictly positive for all  $x \geq 0$  and has a relative minimum at  $m \approx 250$ .

## The Fokker-Planck Equation

The difficulties encountered in trying to solve the master equation have prompted some investigators to seek *approximating* equations in which the state variable  $x$  is regarded as *continuous* instead of discrete. To derive such an approximating equation for equation (3), let the quantity

$$\frac{1}{2}[a_-(x+1)P(x+1,t) + a_+(x-1)P(x-1,t)]$$

be added and subtracted to the right side. A simple rearrangement of terms then yields

$$\begin{aligned} \frac{\partial P(x,t)}{\partial t} = & -[v(x+1)P(x+1,t) - v(x-1)P(x-1,t)]/2 \\ & + \frac{1}{2}[a_+(x+1)P(x+1,t) - 2a_+(x)P(x,t) \\ & + a_+(x-1)P(x-1,t)], \end{aligned} \quad (9)$$

where

$$v(x) \equiv a_-(x) - a_+(x) \text{ and } a(x) \equiv a_-(x) + a_+(x). \quad (10)$$

Now, if  $x$  were a *continuous* variable, the two terms on the right side of equation (9) would be mutually compatible approximations of, respectively, the first  $x$ -derivative of  $-v(x)P(x,t)$  and the second  $x$ -derivative of  $a(x)P(x,t)$ ; moreover, these approximations should be good provided that  $x \gg 1$ . We thus conclude that an approximate "continuum" version of the master equation (3) is

$$\frac{\partial P(x,t)}{\partial t} = - \frac{\partial}{\partial x} [v(x)P(x,t)] + \frac{1}{2} \frac{\partial^2}{\partial x^2} [a(x)P(x,t)]. \quad (x \gg 1) \quad (11)$$

Equation (11) is called the *Fokker-Planck equation*. If we multiply through by  $x$  and then integrate over  $x$  by parts, we find that  $d\langle x \rangle/dt = \langle v(x) \rangle$ , in agreement with equation (5). Mathematically, equation (11) is identical to the equation governing a one-dimensional diffusion process, with  $P(x,t)$  playing the role of the molecular density function,  $v(x)$  playing the role of the average molecular drift velocity, and  $a(x)/2$  playing the role of the diffusion coefficient. In the particular case that

$a_{\pm}(x) = a_{\mp}(x) = D$ , equation (11) reduces to the familiar equation  $\partial P/\partial t = D \partial^2 P/\partial x^2$ . The Fokker-Planck equation is an exact equation for certain continuous-state Markovian processes; however, when the states are discrete it must be regarded as an approximation that is good only for single-step processes with  $x \gg 1$ .

## The Simulation Algorithm

In many ways, the function  $P(x,t)$  is more descriptive of an ensemble of walkers than of an individual walker. One way of focusing on an individual walker is to simulate the random walk on a computer. The key to doing this correctly is a function  $p$ , defined by

$$p(\tau, \mu | x, t) d\tau \equiv \text{the probability that, given the walker is in state } x \text{ at time } t, \text{ it will step next to state } x + \mu \text{ in the time interval } (t + \tau, t + \tau + d\tau). \quad (t \geq 0, \mu = \pm 1) \quad (12)$$

Technically speaking,  $p$  is the "joint probability density function" of the random variables  $\tau$  and  $\mu$ . These two variables evidently specify when and to where the walker's next step will be.

We can derive a formula for  $p$  in the following way: Since  $[a_{\pm}(x)dt + a_{\mp}(x)dt] \equiv a(x)dt$  is the probability that the walker will leave its current state in the next  $dt$ , then well known probability arguments imply that  $\exp[-a(x)\tau]$  is the probability that the walker, in state  $x$  at time  $t$ , will remain there during  $(t, t + \tau)$ . Furthermore,  $a_{\pm}(x)d\tau$  is by definition the probability that the walker, in state  $x$  at time  $t + \tau$ , will step to state  $x + \mu$  in the next  $d\tau$ . The probability defined in equation (12) is therefore just the product  $\exp[-a(x)\tau] \times a_{\pm}(x)d\tau$ . Hence,

$$p(\tau, \mu | x, t) = \{a_{\pm}(x)/a(x)\} \{a(x) \exp[-a(x)\tau]\} \quad (\tau \geq 0, \mu = \pm 1). \quad (13)$$

Equation (13) tells us (i) that  $\tau$  and  $\mu$  are mutually independent random variables; (ii) that  $\tau$  is exponentially distributed with decay constant  $a(x)$ ; and (iii) that  $\mu$  has probability  $a_{\pm}(x)/a(x)$  of being equal to  $\pm 1$ . It is relatively simple to "generate" on a digital computer a pair of random numbers  $\tau$  and  $\mu$  according to these specifications. First, we generate two random numbers  $r_1$  and  $r_2$  from the unit-interval uniform distribution; then we take

$$\tau = [1/a(x)] \log(1/r_1), \quad (14a)$$

and

$$\mu = \begin{cases} -1 & \text{if } a_{-}(x) > r_2 a(x), \\ +1 & \text{if } a_{-}(x) \leq r_2 a(x). \end{cases} \quad (14b)$$

The ability to properly generate a random pair  $(\tau, \mu)$  is evidently all that we need to simulate the random walk. Given initial values of the time variable  $t$  and the state variable  $x$ , we (i) evaluate the functions  $a_{\pm}(x)$  and  $a(x)$ , (ii) draw two random numbers  $r_1$  and  $r_2$  from the unit-interval uniform distribu-

tion, (iii) calculate  $\tau$  and  $\mu$  according to equations (14a) and (14b), and (iv) replace  $t$  by  $t + \tau$  and  $x$  by  $x + \mu$ . Repeating this cycle of steps over and over (on a computer), and periodically recording the instantaneous state of the walker, we obtain a "realization" of the random walk process. If the uniform random number generator is "good," the foregoing simulation algorithm is exact with respect to Equation (1); moreover, it is easily extendable to multivariable, multistep random walks.

Figure 2 shows the results of eight separate simulations of the random walk whose  $P_{\pm}$  function is plotted in Figure 1. These simulations demonstrate vividly the significance of the stable states. They also show how the widths of the stable state peaks in the  $P_{\pm}$  curve characterize the range of the spontaneous fluctuations of the walker about these states.

## The Functions $T_{\pm}^{+}$ and $T_{\pm}^{-}$

We let  $t_x$  be a time long enough after the random walk starts that  $P(x, t_x) = P_{\pm}(x)$ , or

$$P_{\pm}(x) = \text{the probability that the walker will be in state } x \text{ at time } t_x. \quad (15)$$

Then we define two functions  $T_{\pm}^{+}$  and  $T_{\pm}^{-}$  by

$$T_{\pm}^{\pm}(x) \equiv \text{the average time, as measured from } t_x, \text{ before the walker first executes the transition } x \rightarrow x \pm 1. \quad (16)$$

We can obtain an explicit formula for  $T_{\pm}^{\pm}(x)$  through the following line of reasoning: equations (1) and (15) imply that  $P_{\pm}(x) \times a_{\pm}(x)dt$  is the probability that the walker will make the transition  $x \rightarrow x \pm 1$  in any  $dt$  interval after time  $t_x$ . This implies that the time interval from  $t_x$  to the first occurrence of the transition  $x \rightarrow x \pm 1$  is an exponentially distributed random variable with decay constant  $P_{\pm}(x)a_{\pm}(x)$ . Since the average of an exponentially distributed random variable is just the reciprocal of its decay constant, we conclude that

$$T_{\pm}^{\pm}(x) = [a_{\pm}(x)P_{\pm}(x)]^{-1}. \quad (17)$$

Equations (17) and (6) together imply

$$T_{\pm}^{\pm}(x) = T_{\pm}^{\pm}(x-1), \quad (18)$$

which says that the curve of  $T_{\pm}^{\pm}$  is just the curve of  $T_{\pm}^{\pm}$  shifted right one unit of  $x$ . It follows that, for most practical purposes, these two functions can be regarded as one and the same.

If we multiply equation (6) by  $a_{\pm}(x)$  and then invoke equation (17), we discover that

$$T_{\pm}^{\pm}(x) = [a_{\pm}(x)/a_{\pm}(x)]T_{\pm}^{\pm}(x-1), \quad (x=1, 2, \dots) \quad (19)$$

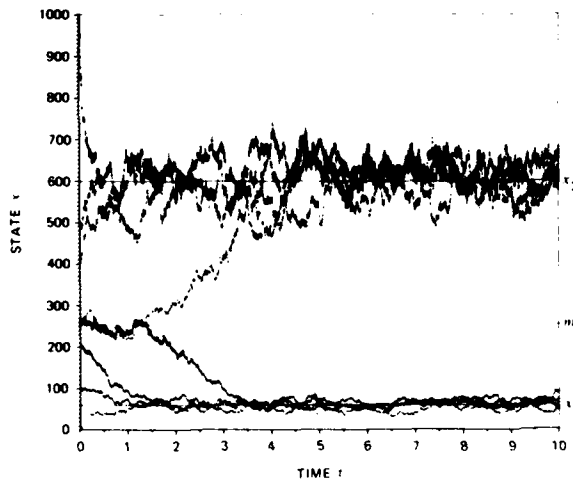
This is a recursion relation for  $T_{\pm}^{\pm}$ , iteration of which yields

$$T_{\pm}^{\pm}(x) = T_{\pm}^{\pm}(0) \prod_{n=1}^x [a_{\pm}(n)/a_{\pm}(n)], \quad (x=1, 2, \dots) \quad (20)$$

The quantity  $T_{\pm}^{\pm}(0)$  can be calculated simply as  $[a_{\pm}(0)P_{\pm}(0)]^{-1}$ . Comparing equations (19) and (20) with equations (6) and (7), we see that the functions  $T_{\pm}^{\pm}$  are just as easy to calculate as the function  $P_{\pm}$ .

**Figure 2**

Eight simulations of the System in Figure 1.<sup>2</sup>



The "derivative" of  $T'_x$  at  $x$  is, using equation (19),

$$T'_x(x) - T'_x(x-1) = T'_x(x)[1 - a_-(x)/a_+(x)]. \quad (21)$$

We see from this that the extrema of  $T'_x$  are those points  $x$  for which

$$a_-(x) = a_+(x), \quad (22)$$

i.e., those points for which the walker is equally likely to step right or left. We also see from equation (21) that  $T'_x$  slopes up or down at  $x$  according to whether  $a_-(x)$  is less than or greater than  $a_+(x)$ . That implies that the walker always has a bias to move "downhill" on the  $T'_x$  curve; moreover, the greater the downward slope, the stronger the bias. The functions  $T'_x$  thus have somewhat the character of a *potential function* for the random walk. In particular, it follows from equations (22), (8), and (17) that the relative minimums of  $T'_x$  approximately coincide with the relative maximums of  $P_x$ , and vice versa. Therefore, the stable states of the system can just as well be defined as the *relative minimums* of the functions  $T'_x$  and  $T_x$ .

The foregoing points are illustrated in Figure 3, which shows a plot of  $T'_x$  for the same system considered in Figures 1 and 2. Because of equation (18), a plot of  $T_x$  would look virtually identical. The  $T'_x$  plot shows much more clearly than the  $P_x$  plot the true nature of the "barrier" at  $m \approx 250$  that separates the stable states at  $x_1 \approx 60$  and  $x_2 \approx 600$ .

## First Passages and Stable-State Transitions

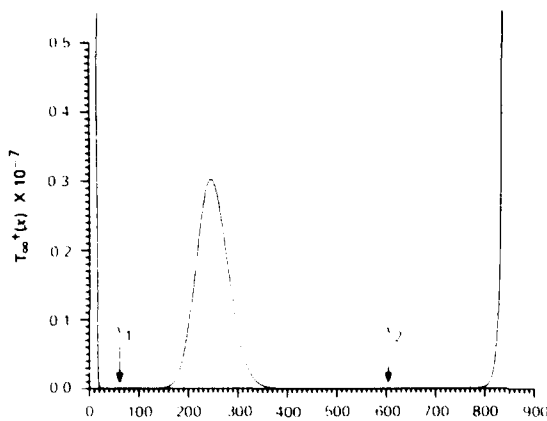
An inspection of Figures 2 and 3 prompts the question of how long it would take a walker initially in one stable-state "valley" to beat the odds and make it over the "hill" into the other stable-state valley. In other words, what is the average time for a *spontaneous transition* from one stable state to another? Such a question could arise in connection with, say, the stability of an electronic memory element against a spurious change of state, or the stability of a living cell against mutation.

Let us pose the problem in a slightly more general way: If the walker starts in any state  $x=u$ , what is the average or expected time  $t(u \rightarrow v)$  until it first reaches any other state  $x=v$ ? We need not require  $u$  and  $v$  to be stable states, but for the present discussion we shall require that  $v > u$ .

To calculate  $t(u \rightarrow v)$  we first introduce some auxiliary quantities, all defined relative to the walker's "first passage" from  $u$  to  $v$ :  $t(x;u,v)$  is the average total time spent in state  $x$ ,  $n(x;u,v)$  is the average total number of visits to state  $x$ , and  $n_-(x;u,v)$  is the average total number of  $x \rightarrow x-1$  transitions. In our derivation of the simulation algorithm, we found that  $1/a(x)$  is the average time the walker spends in state  $x$  on any one visit; thus,  $t(x;u,v)n(x;u,v) = 1/a(x)$ . We also found that  $a_-(x)/a(x)$  is the probability that the walker, upon leaving state

**Figure 3**

The function  $T_x^*(x)$  for the system of figures 1 and 2.



$x$ , will jump to state  $x \pm 1$ ; thus,  $n_-(x;u,v)/n(x;u,v) = a_-(x)/a(x)$ . Dividing this last equation into the preceding one, we get

$$t(x;u,v) = n_-(x;u,v)/a_-(x). \quad (23)$$

By definition, a first passage from  $u$  to  $v > u$  must have exactly one transition  $v-1 \rightarrow v$ , so

$$n_-(v-1;u,v) = 1. \quad (24a)$$

Also, the number of  $x-1 \rightarrow x$  transitions minus the number of  $x-1 \leftarrow x$  transitions must be exactly zero if  $1 \leq x \leq u$  and exactly one if  $u+1 \leq x \leq v-1$ ; thus,

$$n_-(x-1;u,v) - n_+(x-1;u,v) = \theta(x-u), \quad (1 \leq x \leq v-1) \quad (24b)$$

where  $\theta(z)$  is zero if  $z \leq 0$  and one if  $z > 0$ . Dividing equation (24a) by  $a_-(v-1)$  and equation (24b) by  $a_-(x-1)$ , and then making use of equation (23), we obtain

$$t(v-1;u,v) = 1/a_-(v-1), \quad (25a)$$

$$t(x-1;u,v) = \frac{a_-(x)}{a_-(x-1)} t(x;u,v) + \frac{\theta(x-u)}{a_-(x-1)} \quad (1 \leq x \leq v-1) \quad (25b)$$

Equations (25a) and (25b) constitute a complete recursion relation for the average time  $t(x;u,v)$  the walker spends in state  $x$ . Once these times have been calculated for all  $x$ , we can then compute  $t(u \rightarrow v)$  as their sum:

$$t(u \rightarrow v) = \sum_{x=u}^v t(x;u,v). \quad (26)$$

Equations (25a), (25b), and (26) lend themselves nicely to numerical calculations of  $t(u \rightarrow v)$  on a digital computer for explicit functions  $a_+$  and  $a_-$ ; in that way, one can show for the model in Figures 1-3 that the average time for the stable state transition  $x_1 \rightarrow x_2$  is  $t(x_1 \rightarrow x_2) = 2.09 \times 10^6$  time units. Analytical calculation of  $t(u \rightarrow v)$  is also possible with equations (25a), (25b), and (26). For example, for the simple case  $a_+(x) = a_-(x) = D$  considered earlier, one can easily show from equations (25a) and (25b) that  $t(r-x;0,r) = x/D$ ; substituting this into equation (26) gives  $t(0 \rightarrow r) = r(r+1)/2D$ . A general analytical iteration of equations (25a) and (25b) is algebraically messy; however, if one invokes the formulas for  $P_x$  and  $T_x^*$  in equations (7) and (17), one can obtain a compact form for  $t(x;u,v)$  that allows equation (26) to be written in the compact form

$$t(u \rightarrow v) = \sum_{x=u}^v (P_x(x) \sum_{n=\max(u,x)}^{v-1} T_x^*(n) - 1). \quad (u < v) \quad (27)$$

Finally, we may note that equation (27) simplifies even further if  $u$  and  $v$  are the stable states of a bistable system. Referring to Figures 1 and 3, and putting  $u = x_1$  and  $v = x_2$  in equation (27), we see that the  $x$ -summation contributes significantly only for  $x$  under the  $x_1$ -peak in the  $P_x$  curve, while

the  $n$ -summation contributes significantly only for  $n$  under the  $m$ -peak in the  $T^*$  curve. Therefore, the average time for a spontaneous transition from one stable state to the other can be well approximated by the product of {the area under the *initial* stable state peak in the  $P_s$  curve} times {the area under the intervening barrier peak in the  $T^*$  curve}—a surprisingly simple result.

## Concluding Remarks

Scientists trained in classical "deterministic" modes of analysis are often ill-equipped to deal with the uncertainties inherent in nondeterministic systems. For these systems, neither the relevant dynamic quantities nor the fundamental equations that they obey are obvious, and new perspectives and approaches are needed. Simple random walk models like the one considered here are important, not only because they approximate some real-world systems, but also because they provide a context in which new perspectives and approaches can be developed and tested.

## Bibliography

1. Gillespie, D., "A General Method for Numerically Simulating the Stochastic Time Evolution of Coupled Chemical Reactions," *Journal of Computational Physics*, 22 (1976) p. 403.
2. Gillespie, D., "A Pedestrian Approach to Transitions and Fluctuations in Simple Nonequilibrium Chemical Systems," *Physica*, 95A (1979) p. 69.
3. Gillespie, D., "Approximating the Master Equation by Fokker-Planck Type Equations for Single-Variable Chemical Systems," *Journal of Chemical Physics*, 72 (1980) p. 5363.
4. Gillespie, D., "A Stochastic Analysis of the Homogeneous Nucleation of Vapor Condensation," *Journal of Chemical Physics*, 74 (1981) p. 661.
5. Gillespie, D., "On the Calculation of Mean First Passage Times for Simple Random Walks," *Journal of Chemical Physics*, 74 (1981) p. 5295.
6. Gillespie, D., "A Function Useful for Analyzing Single-Step One-Dimensional Markov Processes," *Journal of Chemical Physics*, 76 (1982) p. 3762.
7. Landauer, R., "Stability in the Dissipative Steady State," *Physics Today* (November 1978) p. 23.
8. Matheson, I., D. Walls and C. Gardiner, "Stochastic Models of First-Order Nonequilibrium Phase Transitions in Chemical Reactions," *Journal of Statistical Physics*, 12 (1975) p. 21.
9. Seshadri, V., B. West and K. Lindenberg, "Analytic Theory of Extrema. III. Results for Master Equation with Application to Unimolecular Decomposition," *Journal of Chemical Physics*, 72 (1980) p. 1145.
10. Weiss, G., "First Passage Time Problems for One-Dimensional Random Walks," *Journal of Statistical Physics*, 24 (1981) p. 587.

## Author



Daniel T. Gillespie received his B.A. from Rice University in 1960 and his Ph.D. (Physics) from Johns Hopkins University in 1968. In 1971, after spending three years as a postdoctoral research associate at the University of Maryland's Institute for Molecular Physics, he joined the Research Department of the Naval Weapons Center, China Lake, California, as a research physicist. He is now head of that department's Applied Mathematics Research Branch. His current research interests are in kinetic theory, applied stochastic process theory, and Monte Carlo methods.

# Research Notes

## Healing of Propellant Damage

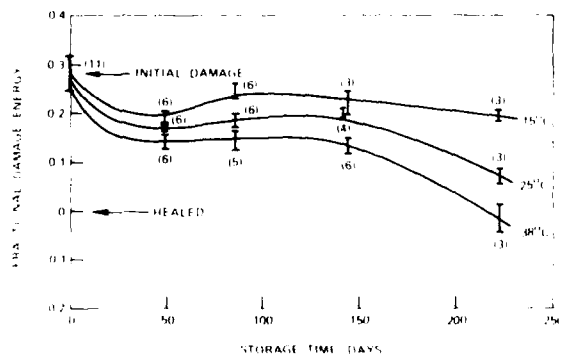
NWC studies of the damage-healing phenomena of solid rocket propellants indicate that at least partial healing of propellant damage occurs within a short time after the damage is introduced. The results of these studies are applicable to the rocket motor service-life prediction program under development.

Composite rocket propellants are highly filled polymers with up to 88% filler consisting mainly of oxidizers. Any finite deformation of a propellant can cause damage to its microstructure in the form of molecular chain scissions and interfacial debonding or dewetting. A damage energy criterion developed at NWC was applied to examine the healing phenomenon of propellant damage. (For more details, see *Journal of Applied Polymer Science*, Vol. 23, 1979.)

Samples of both unplasticized and plasticized propellants were predamaged to various strains and stored at three different temperatures. Several sample withdrawals were made and the remaining damage was determined as a function of time up to 223 days. Some typical results are illustrated in Figure 1.

**Figure 1**

Fractional damage energies versus storage time at three temperatures of plasticized propellant Mk 56B. Numbers in parentheses indicate number of specimens tested.



The healing rate or decrease in damage energy is highest during the first few weeks after damage and increases with the storage temperature. The healing then ceases for a longer time period and even reverses at lower storage temperatures before it finally continues. The unplasticized propellant showed faster healing properties than did the plasticized propellant.

The results of the study indicate that, while at least partial healing of damage occurs, the decrease in damage energy with time and temperature cannot be described by a simple kinetic law over a longer time period. The breaking of molecular chains is a major contributor to damage. The free radicals formed are reactive species and are expected to have short

lifetimes because of the presence of oxygen and other ingredients such as plasticizers, inhibitors, or chain-transfer agents. Therefore, the conclusion can be reached that the healing involves a number of chemical reactions that result in secondary molecular bonds, which then form new primary bonds that can support a mechanical load.

The above considerations suggest that healing takes place within a short time after the damage is introduced into the propellant. The experimental results confirm rapid changes in the propellant's damage level at the beginning of the healing period. The initial modulus recovers 100% as the damage energy approaches zero. However, the ultimate properties of the "healed" propellant are changed—the stress at failure is slightly increased and the strain at break reduced, compared with the baseline properties. Further property changes in the same direction occur as the propellant undergoes further aging.

(Albert H. Lepic, NWC)

## Analytical Chemistry and Pollution Abatement

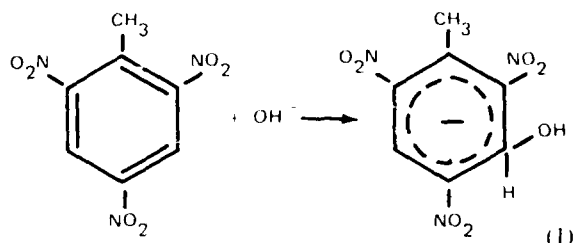
Over the years Naval Weapons Center (NWC) chemists have synthesized, analyzed, and studied a number of new high-energy chemical compounds for use in propellants, explosives, and pyrotechnics. One recent research effort led to the production of a small analytical kit to help the Department of Defense monitor the pollution levels of trinitrotoluene (TNT) and ammonium picrate (AP) at naval bases where these explosives were once dumped. These explosive compounds can seep into water tables and appear in well water where even 10 parts per billion is toxic.

The chemical pollution-detection method developed at NWC depends upon complex chemistry, but the final package is a small kit that can be used by an engineer, technician, or sailor who knows nothing about chemistry. The kit contains a syringe pump and glass tubes filled with the detector chemicals. A given volume of water is pumped through the indicator tube, and a color appears as the water passes through the tube. The length of the color section measures the concentration of TNT in the water. The tubes are expendable, and tubes of different diameter are used for different concentration ranges. Doubling the given amount of water doubles the color length for a given concentration. A solution of known TNT concentration is included in the kit for calibration of the length of the colored section obtained versus the concentration of the known solution.

The chemistry is interesting and depends upon the formation of Meisenheimer anions. These colored anions are then trapped at cationic sites on the surface of ion-exchange resins.

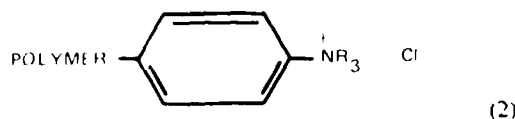
## Research Notes

The structure of Meisenheimer anions is not completely certain, but present evidence would suggest the following chemistry:



This structure is now favored over a structure with one proton removed by the hydroxide anion. Evidence from NWC work suggests that the anions may form dimers and larger polymers that block the resin pores. Various size polymers may account for color variations from red to purple.

The resin is chemically a polystyrene chain with side groups of phenyl rings having tertiary amine groups. This chemistry is depicted as:



The chloride anion is replaced by the more firmly bound Meisenheimer anion. In the case of AP, it is the yellow picrate anion that displaces the chloride anion. NWC researchers are studying methods to alter and intensify the color of the picrate ion.

The chemical reaction (1) is carried out in a short section of the tube filled with a mixed alkaline-earth oxide section. Here the pH is high enough to drive all of the TNT to form Meisenheimer anions. Originally, this section contained only CaO, but the ionic strength of NaCl in brackish water prevented the formation of Meisenheimer anions. Now, with the addition of CaO, SrO, and BaO, the tubes can be operated in areas such as the tidal flats of Virginia.

Environmental engineers have long used color indication tubes for detecting air pollutants, but tubes for detecting water pollutants are a new tool in their arsenal. With this basic idea now established, it is likely that similar tubes to detect other pollutants will be developed for DOD.

(Carl A. Heller, NWC)

## Organometallic Precursors for the Production of Mercury and Cadmium Tellurides

Researchers at the Naval Weapons Center (NWC) are investigating the use of organometallic precursors for the production of II-VI semiconductors in general and for mercury and cadmium tellurides specifically. The use of these organometallic precursors is being pursued for the preparation of thin-film semiconductors with the desired stoichiometry (ratio of numbers of atoms of mercury, cadmium, and tellurium to each other) and purity over large areas.

Infrared sensors constructed of thin crystalline films of mixed mercury-cadmium telluride deposited on a substrate of single-crystal cadmium telluride have the advantage of being able to operate in two different atmospheric windows. The thin films must be of high chemical purity and must be applied to substrates as free from crystalline defects as possible; the stoichiometry of the films must be closely controlled, and the film must be uniform over the entire surface. Further, the films may need to be deposited over larger and larger areas as new requirements for infrared sensors and other semiconductor-film devices arise.

To meet requirements for high purity and closely controlled stoichiometry over large areas, NWC is investigating and developing techniques using organometallic precursors to prepare semiconductor compounds.

The first step in the preparation of semiconductors using organometallic precursors involves the synthesis and characterization of specific model compounds. The model compounds of immediate interest are represented as  $RMXR'$  ( $M = \text{Zn, Cd, or Hg}$ ;  $X = \text{S, Se, or Te}$ ;  $R$  and  $R' = \text{organic groups}$ ). The use of these compounds is a unique approach to the preparation of II-VI materials; they have the required stoichiometry and a metal-chalcogenide bond has already been formed. In fact, they are similar to intermediates postulated during chemical-vapor deposition of semiconductors. Compounds of this type may be purified chemically to almost any desired level of purity.

NWC chemists have prepared  $\text{C}_2\text{H}_5\text{ZnSC}_4\text{H}_9$ ,  $\text{C}_2\text{H}_5\text{CdSC}_4\text{H}_9$ ,  $(\text{C}_6\text{H}_5\text{Se})_2\text{Hg}$ ,  $\text{C}_6\text{H}_5\text{HgSeC}_6\text{H}_5$ , and  $(\text{C}_6\text{H}_5\text{Te})_2\text{Hg}$ , and have also attempted to synthesize  $\text{C}_6\text{H}_5\text{HgTeC}_6\text{H}_5$  and  $\text{C}_6\text{H}_5\text{CdTeC}_6\text{H}_5$ . Although the latter two compounds have not been fully characterized, compelling evidence exists that the attempts have been successful.

Another aspect of the Center's work is the use of light (photolysis) or of temperatures below  $100^\circ\text{C}$  to cause decomposition of the model compounds and formation of the II-VI semiconductor material. The use of these relatively mild conditions (temperatures as high as  $900^\circ\text{C}$  are employed in other decomposition methods) greatly reduces the migration of ions in the crystalline materials and should be a useful technique when devices of these materials are manufactured. The formation of HgSe, HgTe, and CdTe under the mild conditions described has been observed at NWC.

The HgSe was prepared by photolysis of  $C_6H_5HgSeC_6H_5$ , dissolved in a nonaqueous solvent, at room temperature. A broadband ultraviolet source was used, and oxygen was rigorously excluded. Under the same conditions  $(C_6H_5Se)_2Hg$  and  $(C_6H_5Te)_2Hg$  showed no photolytic reaction, although in the presence of sunlight and oxygen from the air the  $(C_6H_5Te)_2Hg$  reacted to give  $(C_6H_5)_2Hg$  and some complex organic tellurium oxides.

The HgTe and CdTe were prepared from the putative precursors  $C_6H_5HgTeC_6H_5$  and  $C_6H_5CdTeC_6H_5$ . The HgTe was prepared by heating benzene or tetrahydrofuran solutions to about 80°C, and also by photolysis at about 30°C under the previously mentioned conditions. The CdTe was prepared by decomposition at room temperature.

(Wayne E. Thun, NWC)

### The Role of Energetic Polymers in Propellants and Explosives

There is an ever-increasing need to enhance the performance of energetic materials, particularly propellants and explosives, in both military and non-military applications. Typical rocket propellants and plastic-bonded explosives (PBX) contain binders of inert polymers. While the inert binders desensitize the hazardous ingredients and provide fluidity (during processing), elongation, and tensile strength, they also degrade energy release. Although efforts are being made to develop superior ingredients, stable and compatible compounds that have appreciably more energy than the current ingredients of ammonium perchlorate, cyclotetramethylene tetranitramine (HMX), and aluminum (Al) are unlikely to be developed in the near future. Therefore, the use of energetic binders may be the most logical approach to the attainment of higher performance.

A family of energetic binders (azido polymers) with polyether backbone has been developed that increases the performance of propellants and explosives without degrading safety, processing, and mechanical properties. The binders are easily prepared in the form of pourable liquids in the 2000 to 4000 molecular weight range. Polyethers have desirable rheological properties and tend to be soft and rubbery, a consequence of the tendency for free rotation of the ether oxygen to carbon linkage.

Energetic polymers offer the potential for increasing the burning rate of normally low-burning propellants containing HMX. Mechanical and safety properties can be enhanced because higher volume fractions of polymers can be formulated without degrading performance, a consequence of the increased energy content of the polymer. Studies of rocket propellants of equal performance indicate that the safety properties are improved as the level of HMX is reduced and the energy contribution of the binder is increased by the addition of a more energetic plasticizer.

The results of recent research at NWC are summarized in the following paragraphs.

### Performance

When inert binders are replaced by denser energetic polymers in propellant compositions, performance is enhanced because of the gain in enthalpy release. Since density as well as enthalpy release are involved in the calculated detonation pressure, the denser energetic polymers produce a relatively greater performance increase in explosive composition than they do in rocket propellants.

### Ballistic Properties

Energetic polymers increase the burning rate of propellants and reduce the extent of aluminum agglomeration. Burning rates are generally enhanced as the azido content of the polymer increases.

### Chemical and Thermal Stability

The azido polymers seem to be compatible with the following typical propellant ingredients as: energetic plasticizers containing nitro, fluorodinitro, and nitrate ester groups; oxidizers such as ammonium nitrate and ammonium perchlorate (AP); nitramines such as RDX (a powerful but sensitive explosive) and HMX; burning rate depressants such as oxamide, and fuels such as the thermogenic light metals Al, Mg, etc. The thermal stability of the prepolymers, cured polymers, and propellant and explosive compositions was found to be superior to that of nitrate esters.

### Mechanical Properties

The mechanical properties of a variety of compositions containing energetic polymers, plasticizers, HMX, AP, and Al were determined; and these compositions were found to have excellent elongation and adequate tensile properties. Low glass transition temperatures were exhibited, an indication that the propellants will show good mechanical properties at low temperatures.

### Conclusions

The current results of the continuing investigation have verified the predictions that the use of energetic binders in propellants and explosives will (1) increase energy release, (2) permit ballistic tailorability, (3) enhance safety properties, and (4) improve the mechanical properties of PBXs. There is growth potential for propellants and explosives, as well as the potential for improved energy release in the areas of gun propellants and pyrotechnics.

(Russell Reed Jr., NWC, May L. Chan, NWC, and Richard S. Miller, ONR)

### **Radar Target Imaging and Inverse Vector Scattering**

The signal processing techniques for the detection and tracking of radar aircraft echoes have been thoroughly investigated over the years, and the optimal methods are well known. However, the signal processing techniques for the classification (friend, foe, or neutral) and identification (for example, F-4 or MIG-23) of aircraft targets are still in the early stages of research. The Naval Weapons Center (NWC) is investigating a classification and identification technique that uses the polarization characteristics of the radar echo, along with a modest degree of Doppler processing, to form an image of the convex portions of the aircraft (such as the fuselage or engine pods). Then, by determining the diameter and length of the image (or perhaps by extracting other measurements from the image), the type of aircraft can be identified.

This technique employs a direct attack on the solution of the inverse scattering problem by using the vector nature (polarization) of the echo signal. This method is in contrast to most current target identification methods, which require a vast file of experimentally taken radar signals on actual targets. That file is then searched for the best match with an unknown radar echo. No such file is required for the NWC technique.

The depolarization of a radar signal by a scattering surface provides a means by which the local curvature properties of the surface may be determined. Furthermore, a classic problem in differential geometry (Christoffel-Hurwitz) deals with the reconstruction of such a surface from a knowledge of this kind of information, and a differential equation relating these local measurements to the surface has long been established. Unfortunately, its exact solution requires an exhaustive amount of input data, more than could be realized by any expected radar encounter.

It is possible, however, to attack not the differential equation but the corresponding variational problem and thereby allow for a solution on a finite data set. In this way, a solution that best fits the known data can be found.

A FORTRAN code employing this "finite-element" inversion algorithm has been constructed and tested on synthetic data. The effect of perturbed or corrupted data on this algorithm has also been investigated, as well as the extent to which the data set can be limited.

Future plans call for evaluating the technique first on a 94-GHz experimental radar at NWC using scale model targets, and then using a suitable polarimetric radar on full-size aircraft targets.

*(Brett Borden and Robert J. Dinger, NWC)*



## Naval Weapons Center

The Naval Weapons Center (NWC) at China Lake, located 150 miles north of Los Angeles, covers a million acres of California's Mojave Desert. In 1943, a Navy and California Institute of Technology team created a thriving scientific facility, known as the Naval Ordnance Test Station (NOTS), in this vast and sparsely populated region. Here the Navy successfully met the urgent wartime need for aircraft ordnance development and testing. The early partnership established a pattern of cooperative interaction between civilian scientists and experienced military personnel that, in the ensuing four decades, has made NWC one of the preeminent research institutions in the country.

Toward the end of the 1940s, NOTS began research on a fire-control system that in time became Sidewinder, the nation's first passive infrared-homing air-to-air guided missile. With the advent of the Korean conflict in 1950, NOTS rapidly gained cognizance over an extensive catalog of air-to-air rockets, guided missiles, air-launched torpedoes, and an array of guns, bombs, and fuzes. By the late 1950s, research expanded into such diverse fields as antisubmarine weaponry and weather modification.

American involvement in Vietnam in the 1960s quickened the tempo of activities at NOTS, and a new generation of "smart" bombs, cluster weapons, and night attack systems was developed. Electronic warfare received major attention, and the Station also made important technical contributions to Navy electronic countermeasures and counter-countermeasures capabilities.

In 1967, NOTS and the Naval Ordnance Laboratory, Corona, joined to form the Naval Weapons Center. The Center acquired the National Parachute Test Range (NPTR) function in 1979 and now serves as a national parachute test-and-evaluation facility.

Today, NWC carries out the complete development process—from basic research to prototype hardware to test and documentation—on over 800 separate programs or tasks. The Center's major programs include: Sidewinder, Sparrow, and Phoenix air-to-air missiles; Harpoon and Walleye air-to-surface weapons; the high-speed antiradiation missile (HARM); fuel-tank recovery parachutes for the space shuttle; and avionics support for a variety of tactical aircraft.

**DAT  
FILM**